NATIONAL TECHNICAL UNIVERSITY OF ATHENS

DIPLOMA THESIS

Speed and Load Dependent Ball Bearing Dynamics in Elastohydrodynamic Lubrication Regime and Application in Jet Engines

Author:
Ino Stylianopoulou

Supervisor:
Athanasios Chasalevris

A thesis submitted in fulfillment of the requirements for the degree of Diploma in Mechanical Engineering

Athens, February 2024

Contents

List of Figures

List of Symbols

The meanings of the following symbols may vary, however, they are explained within the text. Matrices are generally expressed as bold uppercase characters. Vectors, are mentioned as such within the text. Units of each element may vary, according to the given example. Such cases, will be indicated accordingly.

Latin Symbols

A	m	Inner and outer raceway curvature centres distance
b	m	Elliptical half axis of the transverse direction
$\mathbf{C}$		Damping matrix
c		Physical(dimensional) damping
D	m	Diameter
E	Pa^2	Young's modulus
E_p	N/m^2	Prime Young's modulus
E_{red}	N/m^2	Reduced Young's modulus
$\mathbf{F}$		Force vector
F	N	Force
F_z	N	Centrifugal force
h_0	m	Lubricant film height
J	kgm^2	Moment of inertia
$\mathbf{K}$		Stiffness matrix
K_H	$N/m^{1.5}$	Hertzian parameter
L		Dimensionless Moes parameter
$\mathbf{M}$		Mass matrix
M		Dimensionless Moes parameter
M_g	Nm	Gyroscopic moment
m_b	kg	Mass of rolling element

N		Number of balls
P	Pa	Stress
Q	N	Elastic force
r	m	Radius
u	m	Inner ring displacement vector
v	m/s	Circumferential velocity
x, y	–	Axes radial direction
z	–	Axis along axial direction (engine rotation axis)

Greek Symbols

α	m	Elliptical half axis of the direction of motion
α_0	rad	Unloaded contact angle
α_k	rad	Loaded contact angle at position k
α_L	m	Axial clearance
α_p	Pa^{-1}	Pressure-viscosity coefficient
δ	m	Elastic deformation
$\mathcal{E}$	-	Second kind elliptic integral
η	–	Grekkousis approximation parameter
η_0	–	Dynamic viscosity at ambient pressure
θ	rad	Ball pitch angle
κ	–	Ellipticity parameter
λ	–	Race control parameter
ν	–	Poisson's ratio
ξ	–	Grekkousis approximation parameter
ρ	m	Curvature radii
ϕ	rad	Circumferential position of rolling element
ϕ_0	rad	Initial angular position of rolling element
ψ_x, ψ_y, ψ_z	–	Rotations along x-, y-, z-axis
ω_b	rad/s	Rolling element's rotational speed
ω_c	rad/s	Cage's rotational speed

Ω	rad/s	Rotor speed

Subscripts and Superscripts

$(...)_{\mathrm{b}}$	Referring to rolling element
$(...)_{\mathrm{c}}$	Referring to cage
$(...)_{\mathrm{in}}$	Inner
$(...)_{k}$	Referring to the number of ball
$(...)_{\mathrm{out}}$	Outer
$(...)'$	Derivative with respect to position
$\dot{(...)}$	Derivative with respect to time

Abbreviations

DoF	Degree of freedom
EHD	Elastohydrodynamic lubrication
LP	Low-pressure

Acknowledgments

I would like to express my deepest appreciation to my supervising professor, Athanasios Chasalevris of National Technical University of Athens for giving me the opportunity to work in this project and pushing me to the best of my abilities. I would also like to express my deepest gratitude to my supervisor Dr. Christian Wagner, who supported me and this project with his guidance.

In addition, special thanks go to Dr. Ioannis Chatzisavvas, as many times he shone his lights in many parts of the project, as well as giving me the right advice. It has been a great privilege and honour to work under experts of that field and gain many valuable experiences during that process. I would like to acknowledge my fellow classmate Vasileios Veloudis, who has helped me extend the bounds of this thesis. I would not remiss in not mentioning MTU Aero Engines AG and the Rotordynamics team as a whole, for providing me with the opportunity to produce this work. Special thanks go to my fellow students at the company that provided me with help, whenever was needed.

I would also like to give special thanks to my parents for raising me to be curious, resilient and pushing me to pursue my dreams. In addition, I am really grateful for them for introducing me to sciences from an early age, breaking gender stereotypes and putting me in a road of ethos. Special thanks go to my sister Lydia too, who has been a rock of support for me during this stage of my life and who I look up to. Thank you for being there when I needed you the most.

To my new friends in Munich, it has been a pleasure meeting you and making this whole experience even more enjoyable. Special thanks goes to Antreas, who has always lent me his advice and experience, whenever I needed him. To my university friends, both Cypriot and Greek, thank you for being my fellow travellers to this academic experience. Special thanks go to my dear friends Mariza, Kalypso and Evi for being there for me during difficult times. To my close friends back in Cyprus, Nika, Despina, Alex, Eytixia, thank you so much for being by my side for so many years, even though we were divided by distance. Your company always gave me strength in difficult times. Special gratitude goes to two women that I looked up to, Lena and Suzanna, who have really led me to become a better version of myself. Lastly I would like to thank God, for helping me get through all the difficulties and emerging stronger, while experiencing His guidance everyday.

1 Introduction

1.1 Jet Engine Outline

Aircraft engines, often referred to as jet engines are the heart and soul of modern aviation. In general, jet engines, generate thrust by the usage of jet propulsion. These propulsion machines are the reason for the revolution of travel philosophy in the past century. Modern air crafts are able to to soar through the skies at unprecedented speeds and altitudes, for a substantial time, withstanding various weather conditions. In this part of the introduction we will delve into the fascinating world of jet engines, exploring their fundamental principles which made them a pivotal part in the world travel. Two books that have summarized beautifully the dynamics behind jet engines are written by Friswell [4] and Geradin [6]. Here are the main components of a typical jet engine, which work together expelling high-velocity exhaust gases and powering the aircraft:

- Inlet: Also known as the air intake, it's the front part of the engine that captures and compresses incoming air.
- Compressor: It contains multiple rotating blades, which compress the incoming air, by increasing its pressure before it enters the combustion process.
- Combustion Chamber: In this area, fuel is injected and mixed with the compressed air. Then the mixture that is created is ignited, as a result creating high-pressure.
- Turbine: Turbines are then driven by the high-pressure gases. These turbines extract energy from the gases to provide thrust.
- Exhaust Nozzle: In this rear part of the engine, high-velocity exhaust gases are expelled, creating thrust to power the compressor and the fan by the shafts.
- Accessory Gearbox: This component powers accessories such as generators, hydraulic pumps and auxiliary systems

The following figure presents the positions of bearings that are being used in the Rolls-Royce Trent 1000 engine:

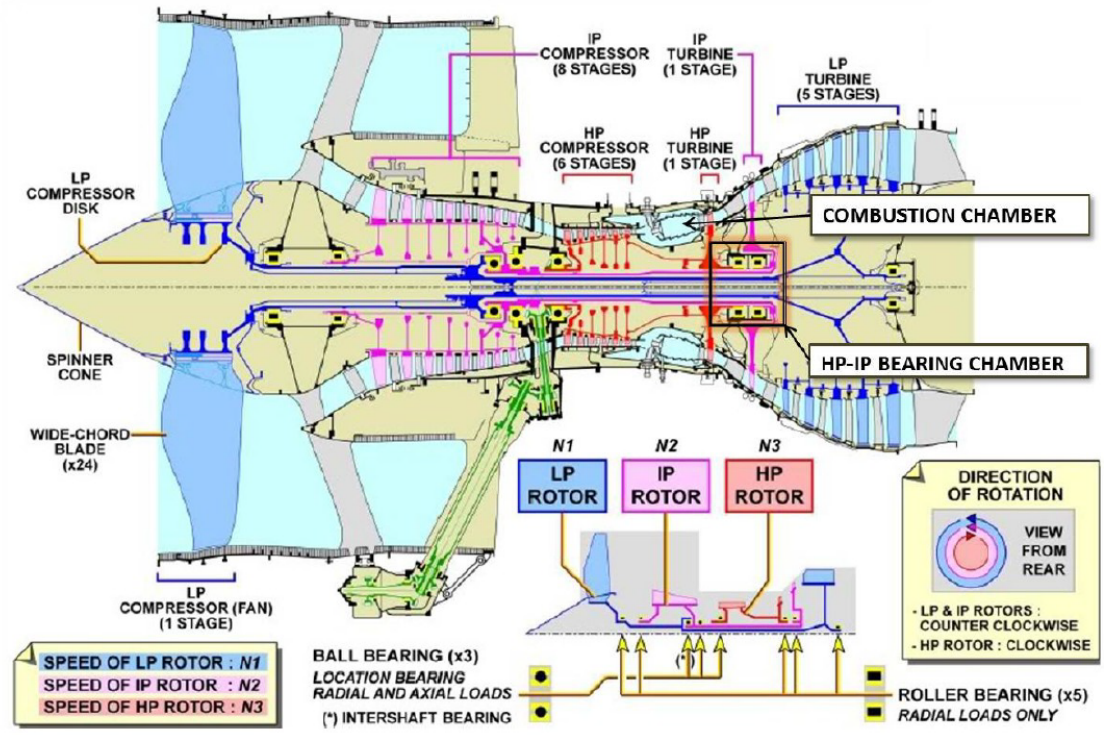

Figure 1.1: Bearings of the Rolls-Royce 1000 Engine [22]

1.2 Bearing Applications in Jet Engines

Bearings in general play a crucial role in jet engines, ensuring their smooth and efficient operation. More specifically, ball bearings are widely used in this field, due to their ability to substain high trust loads and speed, while maintaining a low cost. Here are some key applications of ball bearings in jet engines:

- Compressor and Turbine Bearings: Ball bearings are used to support the rotation of the compressor and turbine blades, which operate at very high speeds and temperatures. Ball bearings allow precise alignment and reduce friction, which is an essential element for the efficiency of the compression and expansion of air and gases within the engine.

- Accessory Drive Bearings: Accessory drives power systems like hydraulic pumps, generators and fuel pumps. The shafts of these drives are being supported by ball bearings, that ensure their smooth rotation

- Thrust Support Bearings: Jet engines generate an enormous thrust to propel the aircraft forward. Ball bearings are design this way to withstand this thrust and support axial loads, handling the forces generating during take-off and flight. These bearings help maintain the axial position of the engine's rotating components

- Auxiliary Power Unit Bearings: These units are smaller gas turbine units and they are used to provide auxiliary power for functions like starting the main engines,

electricity generation and air conditioning. In these systems ball bearings are used to support the shafts

- Gearbox Bearings: Ball bearings are often used in gearboxes, to ensure an efficient power transmission and reduce wear.
- Variable Geometry Bearings: In the case that a jet engine carries variable geometry components, e.g. adjustable guide vanes or nozzle vanes, ball bearings are used to support that movement to ensure a precise control of airflow and thrust.
- High-Speed Bearings: Ball bearings are optimal to withstand the extremely high operating speeds of ball bearings, with minimal friction and wear. Not only that, but they are made in such material to even operate in extremely high temperatures.

In conclusion, ball bearings are essential components in jet engines, contributing to their reliability, efficiency, and overall performance. These small but essential parts of the whole machine help reduce friction and wear, ensure the precise operation of critical engine components, allowing for precise control of airflow and thrust.

1.3 State of the Art

Mechanisms that require transfer of rotary motion are in need of a machine element that permits such motion, allowing such power transmission. A common practice throughout the years, is the usage of bearings. Specifically, ball and roller bearings, often referred to as "rolling bearings", are preferred, for their ability to establish a good power transmission and load support, with minimum power losses and lubrication cost. For that reason, it is now a common practice to use ball bearings, amongst other bearings, in other complex mechanisms such as jet engine rotors. To ascertain what a fundamental part bearings play in modern engineering applications, it is essential to understand how these bearings operate and can withstand operating under strenuous operations, such as a jet engine environment.

Most information about bearings are available from the manufacturers, who present data usually extracted from tests or purely out of empirical nature. Either source of information is often given from the American National Standards Institute (ANSI) or International Organization for Standards (ISO). However, that data only present applications which involve mostly low speeds, low loads and low temperatures. In order to fully take advantage of the potential of bearings, an engineer needs to return to the basics.

A very thorough and overall summation of the potential of rolling bearings is provided by Harris, with the book "Rolling Bearing Analysis" [11]. Harris' book dives deep into the dynamic phenomena that surround the bearing's operation. Harris has managed to keep condensed and simplified the concept and mathematical presentations after thoroughly reviewing the available literature at the time. From the kinematics and motions to lubrication effects and fatigue life. This book is a standard for every engineer that needs to fully grasp the idea of complexity of rolling bearings.

Going back some years, in the 60s, Jones [12],[13] has published some articles that contain details about the elastic constraints and different motions that occur in ball bearing operations. The first publication "Ball Motion and Sliding friction in Ball Bearings" [12], conceptualizes the sliding motions along with the pressure areas. Here, a method is derived to determine the motion of the ball, along with the power loss because of sliding friction. Specifically, the analytical expression of the elliptical pressure of contact is denoted. This paper then is connected with his next publication "A General Theory for Elastically Constrained Ball and Radial Roller Bearings Under Arbitrary Load and Speed Conditions". This paper presents the general equations for the elastic equilibrium of ball bearings. What is notable here, is that this is the first time the term "race control" has been referenced, in terms of literature. In order to solve the equilibrium, a race control type must be assumed. Jones provides with two expression to check the type of race control. However, in order to determine the type, the dynamic operating contacts need to be determined iteratively. These terms are explicit to the ellipse's coordinates, which is a complicated matter by itself. Jones offers the general equations, but the level of complication is that great that in modern ball bearing engineering race control is either ignored completely or defaulted as outer race control (as Harris also supports). Servais and Bozet tried to follow up on this idea with their publication "New computational method of the ball/race contacts transverse loads of high speed ball bearings without race control hypothesis" [24], [23], [2]. Basing their hypothesis on the Jones and Harris ball bearing kinematic theory, they develop a method in determining the type of race control. However, in order for this method to be successful, the different speeds of the ball's contact area with the rings must be determined. Once again, this leads back to Jones [12], with the relative motions of the rolling element. In that regard, Noel [21] introduces another way to determine the power distribution, instead of the race control: The Hybrid hypothesis, which is based on the d'Alembert's principle. His assumption was based on Changan's publication [3].

Lim and Singh provide explicit expressions of non-linear stiffness of rolling bearings, that contain kinematic and elastic characteristics [18], [19]. This paper develops a new mathematical model of the rolling element bearings, while providing with a numerical scheme to compute the stiffness matrix $\mathbf{K}$. Indeed, here a simple computational way of calculating the non-linear forces and stiffness is given. However, the proposed kinematic relations remain quite basic and stay within the premise of a constant Hertzian parameter and a single contact angle. Based on this paper, Wagner [26] further extends the ball bearing modelling. In his thesis he introduces new kinematics that take into account the different contact angles of the rolling element. In addition, the modelling of dry and lubricated contact are introduced. He also takes into consideration the different gyroscopic and centrifugal phenomena. In other words, introducing not only kinematic but also the dynamic modelling of such bearings. Likewise, Wensing [28] thoroughly explains the development of stiffness and damping for both dry and lubricated contacts. In regards of the calculation of the Hertzian area, Grekkousis has done an approximation [7], which the papers use. Additional kinematic relations are given by Wang [27], Liao [16] and Kurvinen [15] but most of them remain in the premise of the kinematics that Harris suggest. In some cases variations are suggested. Liew [17] explores the kinematic relations of a Five-degrees-of-freedom model with inertia and holding a transient solution method for such model. Furthermore, Gao [5] suggests another non-linear dynamic ball bearing model, taking into consideration thermal effects.

Gupta [8] has created a commercial tool for dynamic calculations of bearings, called ADORE [9]. This stand alone tool , however, cannot be coupled directly with a rotor

to execute dynamic simulations and investigate directly the effects of the whole system. In addition, since it is a commercial tool, the kinematics and other modelling of the phenomena are not available to the public. To investigate the effects of a ball bearing coupled with a rotor Tiwari [25] suggests to couple the rotor a bearing using a resultant translational velocity.

1.4 Motivation

Jet engine applications are operating under high speeds and loads. These conditions are producing high thrust loads, making conditions in need of support. In order for the rotor to sustain these loads, supporting structures are introduced, such as bearings. These bearings may be of several types. For large loads, then ball bearings are used. Ball bearings provide a great load support and stiffness, but influence the dynamic behaviour of the whole structure, influencing the natural frequencies of the system. The effect of the load and speed on the bearing's stiffness needs to be investigated, as it is natural that the stiffness does not remain constant during the operation of the jet engine. This dependency can change the system's whole transient response and introduce new excitations in the system. In addition, the modelling non-linear bearings, can lead to completely replace of Squeeze Film Dampers (SFD) in aircraft engines, providing non linear damping, reducing the cost in oil and manufacturing. As of now, aircraft engine rotors are supported by a combination of rolling bearings and SFDs. However, by having a non-linear bearing that provides adapting stiffness and damping, can operate in the rotor, without the help of SFD damping.

Furthermore, there are no commercial tools available that have implemented non-linear stiffness, while investigating the effects by directly coupling the model to a jet engine rotor. Implementing non-linear ball bearings can give us a clear view on the kinematics that are being used and develop more advanced modelling methods to provide even more accurate results. The purpose of this thesis is to provide the reader with a structured idea of the steps that are taken to create such advanced modelling. Specifically, the current thesis deals with the speed and load dependency of both kinematic and dynamic modelling, taking into consideration different phenomena, e.g. elastohydrodynamic lubrication, gyroscopic moment, centrifugal forces etc. In addition, this model is able to directly be coupled to a jet engine model and provide fast results of time transient responses and harmonic balance with minimum convergence problems. One specific element that sets this thesis apart, is the introduction of the race control hypothesis implementation. All in all, the models that are being introduced can be further extended to other types of non-linear bearings, such as roller bearings, or having additional implementations such as thermal effects, skidding, press fits.

1.5 Content of Chapters

In Chapter 2, there is an overview of the modelling that will follow. The distinction between Kinematic and Dynamic Modelling is made, along with a brief information of

the basic content of each model. In addition, the inverse and direct formulations are also introduced.

Chapter 3, takes a dive into the theoretical background of the kinematic modelling. The bearing's geometry is introduced along with the kinematic relations. This chapter thoroughly explains how the dry and lubricated contacts are modelled accordingly. The explicit expressions that contain kinematic and elastic characteristics are given. All variations of the kinematic modelling are then compared in a separate section.

Chapter 4, presents the formulation of the dynamic modelling. Different variations of kinematic equations are examined. Furthermore, the race control hypothesis is introduced. This hypothesis is further investigated with case scenarios. Ball pitch angle is also discussed with corresponding results.

In chapter 5, validation of the previous models with a commercial dynamic simulation tool (ADORE). Different cases are investigated for the speed and load dependency of the bearing's stiffness. Finally, a realistic example of an aircraft engine's Low Pressure (LP) rotor is used for further validation.

Chapter 6, the coupling of the models with a different rotor examples is examined. This chapter goes into detail on how the coupling is established. Then, the results of the transient simulation are showcased (time domain plot and spectrogram). In the end, the findings are discussed and future work is suggested.

In chapter 7, the conclusion takes place, along with a summary of the principle ideas of the thesis. Further suggestions and future works are also discussed.

2 Bearing Theory

2.1 Introduction to Bearing modelling

This particular thesis focuses on the modelling of ball bearings under high speed and loaded conditions. A group of different modelling formulations will follow, as additional changes and different phenomena are added gradually. There are two big distinctions that are made: Kinematic and Dynamic modelling. Both the models provide non-linear stiffness, however, each have a series of phenomena that they either neglect or take into consideration. It is up to the user to determine what model is fit for each operation.

The models that fall under the basic category of Kinematic modelling, follow the Lim and Singh [18] kinematic formulation of ball bearings. They hold the same approach when it comes to the calculation of the contact angle α_k and they neglect any centrifugal forces and gyroscopic moments. They follow a dry Hertzian contact or a lubricated contact. Skidding and rolling phenomena are neglected. All in all, there is an implicit connection from the kinematics to the calculation of stiffness. Damping is provided only for the lubricated case.

The ball bearings that follow the dynamic modelling have different contact angles for the ball raceways (α_{out},α_{in}) and take into account the additional degrees of freedom (DoFs) of the ball, as well as the centrifugal forces. they solve the dynamic equilibrium each time and they apply the race control hypothesis. The calculation of the stiffness and forces is now provided by solving numerically the problem, while load and speed conditions are directly introduced into the problem.

2.2 Forward vs. Inverse Formulation

There are two different problem formulations, that can provide different solutions depending on the wanted outcome. An inverse formulation, is expressed by applying a known force, thus acquiring the displacement of the inner ring, by solving the quasi-static equilibrium. Alternatively, a forward or direct problem was given the inner ring displacement and then calculates the occurred force, following analytical expressions. The following results are mostly generated by using the direct formulation. However, an inverse formulation was also achieved by approximating the displacement with a solver ("fsolve" in Python). The following parts contain a brief summary of the steps that were followed, in order to produce results, before going in depth in the whole process.

Forward Formulation

As mentioned above, the main idea is that the generated inner ring forces can be determined from the given inner ring displacement. Firstly, global inner ring displacements must be given. Then, based on certain kinematic formulations and the bearing geometry, the axial (u_a) and radial (u_r) displacements are calculated. Also, the individual position of each ball ϕ_k is determined. At this point it must be highlighted that there is a direct correlation between the kinematic formulations, that are being used, and the generated force and stiffness matrices. Thus, making the modelling kinematically sensitive. This relation between the initial inner ring displacement is what also makes the model, load dependent. After more in between calculations are done, the Hertzian parameter K_H must be determined. Later on, it will be proven that this parameter is also dependent on the inner ring displacements. Using this parameter, the theoretical elastic deformation of the ball raceway contacts δ_k and certain projection vectors, the external forces and moments of the inner ring can be determined. Finally, the procedures for determining the stiffness matrix vary, according the calculation method (analytically, numerically).

Inverse Formulation

The inverse problem formulation, follows the exact opposite structure as the forward problem. Meaning, it is given the external load and it returns the inner ring displacement vector u. In order for this to be done, the state vector u must be approximated numerically, for the minimization of the resulting inner ring forces. Of course, an initial vector u must be set in order for this method to work. A later example will showcase this method thoroughly. Using this initial step, we proceed with the calculation of the kinematics and the generated forces and stiffness, for said displacement. In essence, the same steps as the forward problem are applied. However, after the end of the calculation, a minimization of the resulting force follows, using a solver (”fsolve” in Python). Thus, we retrieve the correct displacement that creates said inner ring force and then we proceed with the calculation of the correct force. In other words, an initial input, returns a force and that force generates the correct state vector, that it will be then used to generate the expected inner ring forces and stiffness. This procedure is more time consuming, as it needs more computational power to minimize the function and essentially performing all the calculations twice.

3 Kinematic Modelling

3.1 Standard Lim and Singh Model

Introducing the first bearing model, that follows the proposed kinematic and geometrical relations of Lim and Singh (LS) [18]. They introduce a comprehensive mathematical model to calculate the bearing stiffness matrix **K**, using basic principles.

This method derives the bearing displacement vector u, that is generated from external loads and bearing preload, and calculates the force **F** and stiffness **K** matrices, respectively. This is referred to as "Inverse" formulation. Two methods of approach are used in this thesis: the Forward and the Inverse problem, as discussed before.

In the standard model, the effects of the force and stiffness matrices are transmitted through basic geometric relations of the bearing and the rolling elements. It is assumed that the angular position between each rolling element is always maintained relative, as the cages are assumed rigid and pin retainers are taking place. Furthermore, any effects of centrifugal forces and gyroscopic moments are neglected. A dry contact is in effect and any lubrication or thermal issues are ignored. For the effects of the dry contact, an effective stiffness coefficient (Hertzian Parameter) K_H, is calculated following the Hertzian Theory. Finally, the standard model achieves the computation of a non-linear stiffness matrix **K**, while presenting the parametric dependence between the kinematics and loads.

3.1.1 Kinematics and Geometrical Relations

The proposed model by Lim and Singh(LS) [18] offers a simple depiction of the bearing kinematics. Generally, the rolling element displacements are expressed through constant bearing parameters. This allows the development of a model that gives the liberty of only manipulating the input externally, meaning the bearing geometry.

The following proposed kinematic relations are taken as is from the Lim and Singh (LS) publications [18]. This study proposes a rolling element bearing stiffness matrix **K** which is suitable for analysis of the vibration transmission through a ball bearing and investigate the existence of the non-linear algebraic bearing equations by describing load-displacement dependency. The LS model, offers a linear vibrating system, making fast and easy calculations of the force, stiffness and damping matrices.

In this section, the kinematic and geometric relations will be as expressed from the LS paper. This first "Standard model", the gyroscopic moment, centrifugal forces and

elastohydrodynamic effect, are not taken into consideration. It is also assumed that no skidding or rolling effects occur. Moreover, a rigid cage and ring is assumed, along with common cage speed. Further on, the different dynamic phenomena will gradually be taken into consideration, thus producing a different result, which will be also evaluated.

Ball Bearing Geometry

This section delves deeper into the bearing geometric relations, that are crucial for the definition of ball geometric relations. To initiate the calculation, the bearing's geometric parameters are needed, which are usually available from the manufacturer. This turns out to be helpful, as the user just needs to change externally the bearing parameters in order to manipulate the results. These parameters are: the inner D_{in} and the outer ring D_{out} diameter. The ball diameter D_b, from which the ball radius b_r can be derived as $b_\mathrm{r} = D_\mathrm{b}/2$. The inner ring raceway diameter d_{in} and the inner groove curvature radii r_{in} must be given from the manufacturer. The same applies for the equivalent quantities of the outer ring d_{out} and r_{out}. After enquiring these parameters, using the following expressions, we can acquire the full geometry configuration of the ball bearing. The pitch diameter can be expressed as: $d_\mathrm{m} = (d_\mathrm{out} + d_\mathrm{in})/2$ and the radial position of the inner race curvature centre as: $r_\mathrm{j} = d_\mathrm{in}/2 + r_{in}$. From the above, the unloaded distance between the inner and outer raceway curvature centres A_0 can be calculated:

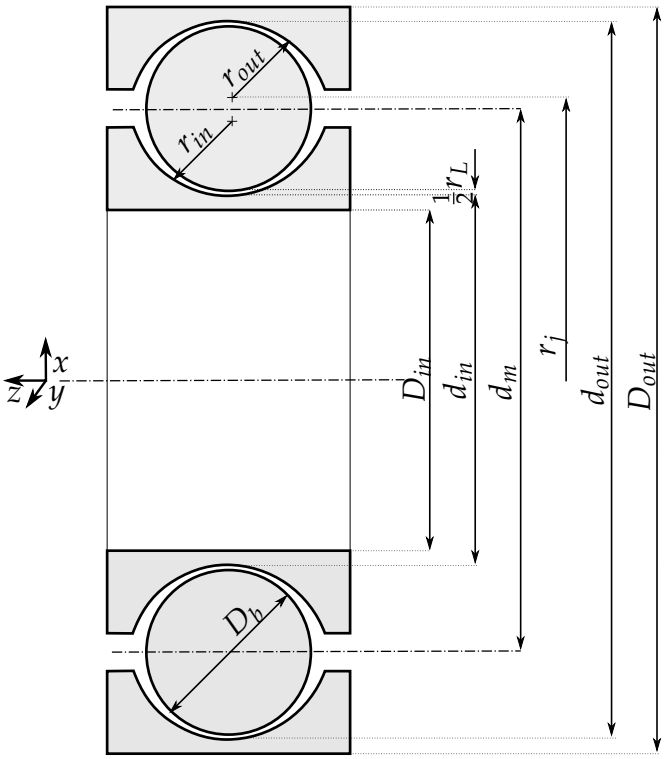

Figure 3.1: Unloaded Bearing Geometry

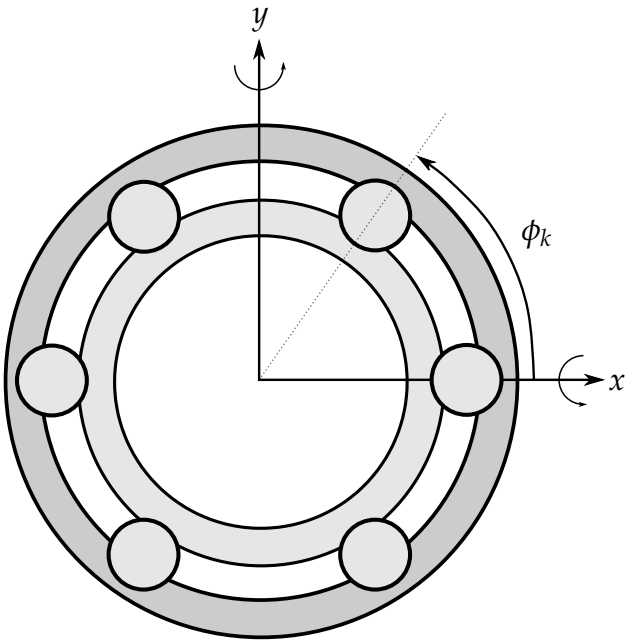

Figure 3.2: Ball Distribution

$$A_0 = r_{\text{in}} + r_{\text{out}} - D_{\text{b}} \tag{3.1}$$

Axial a_L and radial a_r clearance occurs when being in an unloaded state. Meaning, when the bearing is in a force-free state, the axial and radial displacements are expressed as:

$$a_{\text{L}} = A_0 \sin(\text{a}_0), \tag{3.2}$$

$$r_{\text{L}} = r_{\text{in}} + r_{\text{out}} - \frac{D_{\text{b}}}{2} \tag{3.3}$$

where a_0 ,is the unloaded contact angle of the bearing:

$$a_0 = \arccos(1 - \frac{\text{r}_{\text{L}}}{\text{A}_0}) \tag{3.4}$$

As the bearing is in a loaded state and since the outer ring is considered rigid, the rolling elements are distributed evenly. However, different contact angles occur for every rolling element, especially for combined axial and radial loads. According the position of each ball in relation to the loaded zone, the contact angle changes. In order to define that contact angle, first the circumferential position of each individual ball k must be expressed:

$$\phi_k = \frac{2\pi}{N} k + \omega_c t, \quad k\epsilon[0; N-1] \tag{3.5}$$

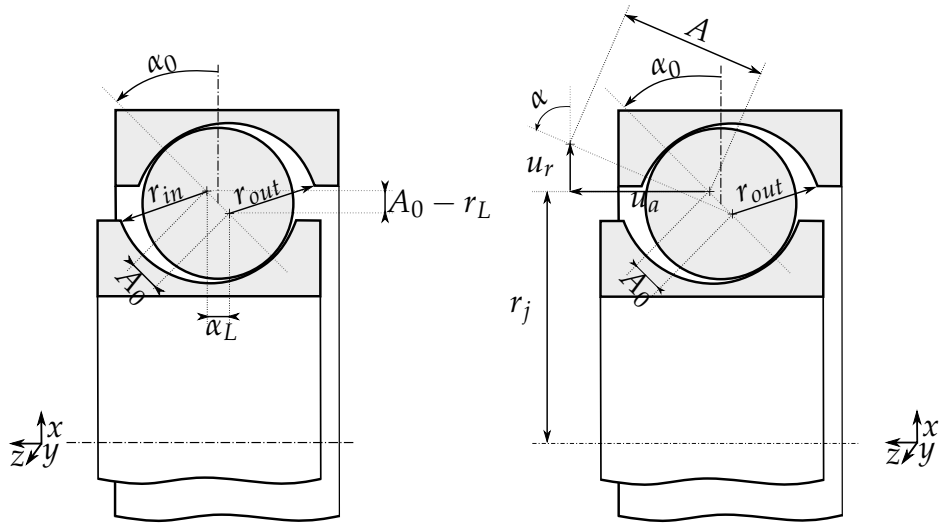

Figure 3.3: Preloaded Bearing Geometry, Inner Ring Displacement

Where ω_c is the rotational speed of the cage. This circumferential position of each element is dependent on the common cage speed ω_c and N the number of balls. This speed is common, as the cage forces the rolling elements to rotate with the same circumferential speed. Once the circumferential position is determined, the axial and radial displacement of the centre of the inner raceway curvature at each balls position k is expressed as [26]:

$$u_{\alpha,k} = u_z + r_j(\psi_x \sin(\phi_k) - \psi_y \cos(\phi_k)), \tag{3.6}$$

$$u_{r,k} = u_x \cos(\phi_k) + u_y \sin(\phi_k) - r_L \tag{3.7}$$

where r_L is the radial clearance, r_j is the radial position of the inner raceway curvature centre and u is the inner ring displacement vector and it is expressed as:

$$u = \begin{bmatrix} u_x & u_y & u_z & \psi_x & \psi_y & \psi_z \end{bmatrix} \tag{3.8}$$

Notably, the displacements above are explicitly dependent on the inner ring displacement vector, making the modelling very sensitive to any movement of the inner ring. Through this, a load dependency can be achieved. It will be discussed later on, that the movement of the inner ring is caused from the load effects that are taking place on the bearing, thus implementing this to the model. It can be also seen, in the previous expressions, that a circumferential position dependency is applied. In this way, a state dependency can be implemented into the modelling.

After the calculation of the bearing's displacements, the elastic deformation of each rolling element follows. Elastic deformation occurs due to the contacts of the rolling elements and the inner and outer rings. In this basic model, a dry Hertzian contact is modelled and the speed effects are neglected. In order to determine this component, the contact angle of each individual ball must be calculated. Within the framework of Lim and Singh, the contact angles between the inner and outer ring are equal ($\alpha_k = \alpha_{in} = \alpha_{out}$). Consequently, the sum of the theoretical elastic deformation is expressed as $\delta_k = \delta_{in} + \delta_{out}$.

First of all, the loaded distance between the inner and outer raceway curvature centres -A_k- must be determined. It expresses the distance between the inner and outer raceway groove curvature centre:

$$dsa_k = u_{\alpha,k} + A_0 \sin \alpha_0, \tag{3.9}$$

$$dsr_k = u_{r,k} + A_0 \cos \alpha_0, \tag{3.10}$$

$$A_k = \sqrt{dsa_k{}^2 + dsr_k{}^2} \tag{3.11}$$

where dsa_k and dsr_k are axial and radial displacements, respectively. Consequently, the loaded contact angle occurs as:

$$\alpha_k = \arctan\left(\frac{dsa_k}{dsr_k}\right) \tag{3.12}$$

and the theoretical elastic deformation δ_k denotes as:

$$\delta_k = \begin{cases} A_k - A_0, & (A_k - A_0) > 0 \\ 0, & (A_k - A_0) \leq 0 \end{cases} \tag{3.13}$$

As shown above, the elastic deformation δ_k consists of the difference between the real (A_k) and the load free (A_0) displacement. Once this value is greater than zero, then contact is established. When, this difference is less or equal to zero, free play occurs. Free play is the phenomenon where the ball is allowed to move freely in the raceway, as it has no movement restriction from contact. Thus when free play is active, no contact force occurs. Thus it is worth noting that there is room for future work in order to improve the configuration of the radial and axial free play, making it more realistic.

There are conditions to which free play occurs [26].

Axial free play:

$$-\sqrt{A_0^2 - (A_0 - 2r_L)^2} - \alpha_L \leq \ u_z \leq \sqrt{A_0^2 - (A_0 - 2r_L)^2} \tag{3.14}$$

Radial free play:

$$-r_L \leq \ u_x \leq r_L \tag{3.15}$$

This shows the restriction of the kinematics by Lim and Singh. The force free radial movement is equal to the free play r_L. The force free axial movement is slightly different to a_L. This is a simplification made by Lim and Singh. This simplification is substituted later, when the updated kinematics are introduced in the Dynamic modelling chapter.

When all the kinematics are implemented, the estimation of the Hertzian parameter follows, as it is necessary for the computation of the elastic normal force $Q_{n,k}$ of each ball:

$$Q_{n,k} = K_H \delta_k^{\frac{3}{2}}, \quad k\epsilon[0; N-1] \tag{3.16}$$

where N is the number of balls.

In order to obtain that, the calculation of the Hertzian parameter must be done.

3.1.2 Hertzian Theory

When the rolling elements and the raceways are respectively in a point contact, due to dry condition, elastic deformation takes place. The geometry of a point contact is described by four radii of curvature. The surface of the inner raceway is convex whereas the surface of the outer raceway is concave. By definition, convex surfaces have positive radii and concave surfaces have negative radii. Due to this concave and convex area contact, an elliptical shape is created. The pressure, known as the Hertzian contact pressure, that is created between the two bodies result in the formation of contact forces. Additionally tangential forces can be transmitted. In later stages of the thesis, the calculation of such forces will be discussed.

3.1.3 Determination of Hertzian Parameters

The calculation of the static normal forces Q_n, occurs with the multiplication of the stiffness coefficient K_H and the elastic deformation due to contact $\delta_k^{\frac{3}{2}}$. As referred in equation 3.13, δ is calculated. The computation for the Hertzian Parameter K_H is done analytically, from the expressions taken from Wensing [28]. In order for the Hertzian Parameter K_H to be calculated, the individual radii of curvature for both inner and outer ring contact must be defined [28]:

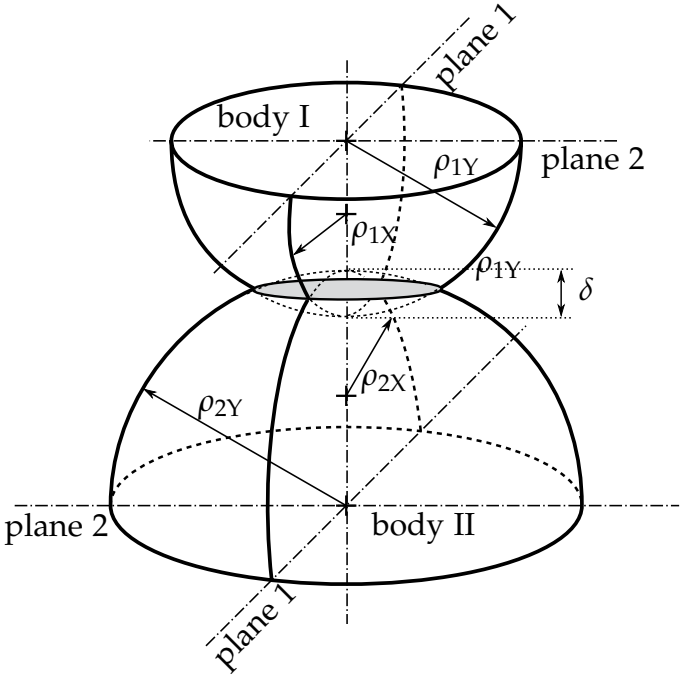

Figure 3.4: Hertz Contact of Two Mounted Surfaces [26]

For inner ring contact:

$$\begin{aligned}
R_{1X,in} &= \frac{D_b}{2}, \\
R_{1Y,in} &= \frac{D_b}{2}, \\
R_{2X,in} &= 0.5\left(\frac{d_m}{\cos\alpha_k} - D_b\right), \\
R_{2Y,in} &= -r_{in}, \\
\rho_{1X,in} &= \frac{1}{R_{1X,in}}, \\
\rho_{1Y,in} &= \frac{1}{R_{1Y,in}}, \\
\rho_{2X,in} &= \frac{1}{R_{2X,in}}, \\
\rho_{2Y,in} &= \frac{1}{R_{2Y,in}}
\end{aligned} \tag{3.17}$$

Similarly, for outer ring contact:

$$\begin{aligned}
R_{1X,out} &= \frac{D_b}{2}, \\
R_{1Y,out} &= \frac{D_b}{2}, \\
R_{2X,out} &= -0.5\left(\frac{d_m}{\cos\alpha_k} + D_b\right), \\
R_{2Y,out} &= -r_{out}, \\
\rho_{1X,out} &= \frac{1}{R_{1X,out}}, \\
\rho_{1Y,out} &= \frac{1}{R_{1Y,out}}, \\
\rho_{2X,out} &= \frac{1}{R_{2X,out}}, \\
\rho_{2Y,out} &= \frac{1}{R_{2Y,out}}
\end{aligned} \tag{3.18}$$

Resulting to a reduced curvature R of the polaroid, for both contacts as:

$$R = (\rho_{1X} + \rho_{2X}) + (\rho_{1Y} + \rho_{2Y}) \tag{3.19}$$

Once the radii are determined, the additional parameter $\cos\tau$, as specified by HERTZ [26]:

$$\cos\tau = \frac{\sqrt{(\rho_{1X} - \rho_{1Y})^2 + (\rho_{2X} - \rho_{2Y})^2 + 2(\rho_{1X} - \rho_{1Y})(\rho_{2X} - \rho_{2Y})}}{R} \tag{3.20}$$

and the function $f(\tau)$ as:

$$f(\tau) = \ln(1 - \cos\tau) \tag{3.21}$$

At this point of the calculation, it is integral to denote the approximation of the parameters ξ and η. These approximations were given by Grekoussis [7] to eliminate time consumption while giving a low error.

$$\ln\xi = \begin{cases} \frac{f(\tau)}{-1.53+0.333f(\tau)+0.0467f^2(\tau)}, & 0 < \cos\tau < 0.949 \\ \sqrt{-0.4567 - 0.4446f(\tau) + 0.1238f^2(\tau)}, & 0.949 \leq \cos\tau < 1 \end{cases} \tag{3.22}$$

$$\ln\eta = \begin{cases} \frac{f(\tau)}{1.525-0.86f(\tau)+0.00993f^2(\tau)}, & 0 < \cos\tau < 0.949 \\ \sqrt{-0.333 - 0.2037f(\tau) + 0.0012f^2(\tau)}, & 0.949 \leq \cos\tau < 1 \end{cases} \tag{3.23}$$

Once these parameters are determined, the first and the second elliptic integrals can be calculated. It must be noted, that the calculation of the integrals is done by using the Grekoussis approximation as the original expressions are denoted as:

$$\mathcal{K} = \int_0^{\frac{\pi}{2}} \left((1 - \left(1 - \frac{1}{\kappa^2}\right)\sin^2\phi)^{\frac{-1}{2}} \right) \mathrm{d}\phi \tag{3.24}$$

$$\mathcal{E} = \int_0^{\frac{\pi}{2}} \left((1 - \left(1 - \frac{1}{\kappa^2}\right)\sin^2\phi)^{\frac{1}{2}} \right) \mathrm{d}\phi \tag{3.25}$$

The approximations for the first and second elliptic integrals are given as:

$$\mathcal{E} = \frac{\eta^3\pi\kappa}{2} \tag{3.26}$$

$$\mathcal{K} = -\frac{\mathcal{E}}{2}(\kappa^2 - 1)\cos\tau + \frac{\mathcal{E}}{2}(\kappa^2 + 1) \tag{3.27}$$

The ellipticity parameter κ is defined as shown below, for each contact:

$$\kappa = \frac{\alpha}{b} = \frac{\xi}{\eta} \tag{3.28}$$

and parameter ζ:

$$\zeta = \frac{2\mathcal{K}}{\pi\xi} \tag{3.29}$$

where α and b ar the half-axis of the contact ellipses, α being the length of the direction of motion, whereas b in the transverse direction.

$$\alpha = \eta \left(Q_n \frac{3E_{red}}{R} \right)^{\frac{1}{3}} \quad b = \xi \left(Q_n \frac{3E_{red}}{R} \right)^{\frac{1}{3}} \tag{3.30}$$

Where E_{red} is the reduced Young's modulus:

$$E_{red} = 0.5 \left(\frac{1 - {v_2}^2}{E_1} + \frac{1 - {v_2}^2}{E_2} \right) \tag{3.31}$$

The $v_{1,2}$ is defined as Poisson's ratio for the equivalent material for each contact body. Similarly, $E_{1,2}$ is the material's Young's modulus. The Q_n for the case of "Dry contact", are the normal forces 3.16.

This flattening of the area, causes a concentration of stresses, hardening the material and thus producing this Hertzian stiffness coefficient K_H. At this stage, material damping also occurs. However, it is quite insignificant and so it is neglected in the present state of the modelling. For inner and outer contact respectively, the following is applied:

$$K_{in,out} = \sqrt{3} E_p \left(\frac{1}{1.5 \zeta R^{\frac{1}{3}}} \right)^{1.5} \tag{3.32}$$

where E_p is the prime Young's Modulus, ζ is given in 3.29 and R is the reduced curvature of the polaroid, for each contact respectively:

$$E_p = \frac{2 E_1 E_2}{E_1 (1 - {v_1}^2) + E_2 (1 - {v_2}^2)} \tag{3.33}$$

Finally, we can proceed with the calculation of the Hertzian stiffness coefficient K_H:

$$K_H = \frac{K_{in} K_{out}}{\left({K_{in}}^{\frac{2}{3}} + {K_{out}}^{\frac{2}{3}} \right)^{\frac{3}{2}}} \tag{3.34}$$

Notice how the above formulation follows the logic that the total Hertzian parameter is the result of each contact's parameter acting as springs in line.

The maximum stress P_{max} of that contact area is as follows:

$$P_{max} = \frac{3 Q_n}{2 \pi \alpha b} \tag{3.35}$$

From all the above, it can be derived that the Hertzian Parameter K_H is heavily influenced by the geometric parameters of the bearing. As a result, two cases are worth investigating: A loaded contact angle α_k or an unloaded contact angle α_0 dependency.

3.1.4 Constant Hertzian Parameter vs. Varying Hertzian Parameter

In this section, an investigation on the effect that the contact angles have on K_H, will be conducted. This will be done by using either the unloaded α_0 or loaded contact angle

α_k, as shown in the individual radii of curvature. When α_k is used, K_H is implicitly dependent to vector u. It is evident that these expressions dependent on the geometry. Specific interest arises concerning the influence of contact angle α_k on the curvature radii. The rest are depended to constant bearing parameters and do not require further investigation. Firstly, this case concerns the unloaded contact angle α_0, cf. eq. 3.4. α_0 is a constant bearing parameter and it is purely dependent to the geometry of the bearing. In this current example, for every step of displacement u_z, there is no effect to K_H. In the case of the loaded contact angle α_k eq. 3.12, K_H is influenced by both the geometry of the bearing as well as the displacement of the inner ring. As it is displayed in figure 3.5 below, the stiffness parameter changes linearly to the displacement.

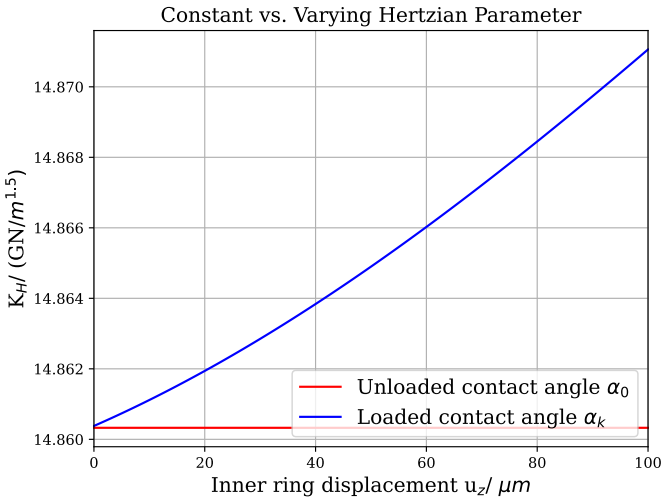

Figure 3.5: Varying and Constant Hertzian Parameter: Comparison for Varying Inner Ring Axial Displacement

As a result, for every step of displacement u_z, a different value for K_H occurs. After investigating this matter, it seems like this variation is almost linear and in general, insignificant. In the grand scheme of the stiffness calculation, which will take part later on, it has almost no effect. Hence, just for accuracy purposes, a loaded contact angle α_k will be used in the more advanced models.

3.1.5 Analytical Expressions of Standard Model

After obtaining the desired K_H using eq. 3.34, the modelling may proceed, by applying the stiffness to the calculation of the recurring elastic forces Q_n (3.16). This modelling follows the analytical expressions as suggested by [26], which are mainly based on the Lim and Singh [18] expressions.

To begin with, the generated inner ring forces are projected to the global coordinates, by using a force projection vector $\mathbf{e}_{f_{LS},k}$, achieving a connection to the global loads $\mathbf{F}$. Thus,

the resulting forces of the inner ring occur as:

$$\mathbf{F} = (F_x \;\; F_y \;\; F_z \;\; M_x \;\; M_y \;\; M_z), \tag{3.36}$$

$$\mathbf{F} = \sum_{k=1}^{N} Q_{n,k} \mathbf{e}_{f_{LS},k} \tag{3.37}$$

,where $\mathbf{e}_{f_{LS},k}$ is the projection vector of each ball-k, to the global inner ring coordinate frame, as given by Lim and Singh [18]:

$$\mathbf{e}_{f_{LS},k} = \left\{ \begin{array}{c} (A_0 \cos a_0 + u_r) \cos \phi \\ (A_0 \cos a_0 + u_r) \sin \phi \\ A_0 \sin a_0 + u_a \\ r_j (A_0 \sin a_0 + u_a) \sin \phi \\ -r_j (A_0 \sin a_0 + u_a) \cos \phi \\ 0 \end{array} \right\} \tag{3.38}$$

The stiffness matrix **K** is produced analytically from these formulations [18]:

$$
\begin{aligned}
k_{xx} &= K_H \sum_{k=1}^{N} \frac{\delta_k^{1.5} \cos\phi_k (\frac{1.5 A_k dsr_k}{\delta_k} + A_k^2 - dsr_k^2)}{A_k^3} \\
k_{yy} &= K_H \sum_{k=1}^{N} \frac{\delta_k^{1.5} \sin\phi_k (\frac{1.5 A_k dsr_k}{\delta_k} + A_k^2 - dsr_k^2)}{A_k^3} \\
k_{zz} &= K_H \sum_{k=1}^{N} \frac{\delta_k^{1.5} (\frac{1.5 A_k ds\alpha_k}{\delta_k} + A_k^2 - ds\alpha_k^2)}{A_k^3} \\
k_{xy} &= K_H \sum_{k=1}^{N} \frac{\delta_k^{1.5} \cos\phi_k \sin\phi k (\frac{1.5 A_k dsr_k}{\delta_k} + A_k^2 - dsr_k^2)}{A_k^3} \\
k_{xz} &= K_H \sum_{k=1}^{N} \frac{\delta_k^{1.5} dsr_k dsa_k \cos\phi_k (\frac{1.5 A_k}{\delta_k}) - 1}{A_{k^3}} \\
k_{x\psi_x} &= K_H \sum_{k=1}^{N} \frac{\delta_k^{1.5} dsr_k dsa_k \sin\phi_k \cos\phi_k ((\frac{1.5 A_k}{\delta_k}) - 1)}{A_{k^3}} \\
k_{x\psi_y} &= K_H \sum_{k=1}^{N} \frac{\delta_k^{1.5} dsr_k dsa_k \cos^2\phi_k ((\frac{1.5 A_k}{\delta_k}) - 1)}{A_{k^3}} \\
k_{yz} &= K_H \sum_{k=1}^{N} \frac{\delta_k^{1.5} dsr_k dsa_k \sin\phi_k ((\frac{1.56 A_k}{\delta_k}) - 1)}{A_{k^3}} \\
k_{y\psi_x} &= K_H \sum_{k=1}^{N} \frac{r_j \delta_k^{1.5} dsr_k dsa_k \sin^2\phi_k (1 - \frac{1.5 A_k}{\delta_k})}{A_{k^3}} \\
k_{y\psi_y} &= K_H \sum_{k=1}^{N} \frac{r_j \delta_k^{1.5} dsr_k dsa_k \sin\phi_k \cos\phi_k (1 - \frac{1.5 A_k}{\delta_k})}{A_{k^3}} \\
k_{z\psi_x} &= K_H \sum_{k=1}^{N} \frac{r_j \delta_k \sin\phi_k (\frac{1.5 A_k ds\alpha_k^2}{\delta_k}) + A_k^2 - ds\alpha_k^2}{A_k^3} \\
k_{z\psi_y} &= K_H \sum_{k=1}^{N} \frac{r_j \delta_k \cos\phi_k (ds\alpha_k^2 - \frac{1.5 A_k ds\alpha_k^2}{\delta_k}) - A_k^2}{A_k^3} \\
k_{\psi_x\psi_x} &= K_H \sum_{k=1}^{N} \frac{r_j^2 \delta_k \sin^2\phi_k (\frac{1.5 A_k ds\alpha_k^2}{\delta_k}) + A_k^2 - ds\alpha_k^2}{A_k^3} \\
k_{\psi_x\psi_y} &= K_H \sum_{k=1}^{N} \frac{r_j^2 \delta_k \sin\phi_k \cos\phi_k (ds\alpha_k^2 - \frac{1.5 A_k ds\alpha_k^2}{\delta_k}) - A_k^2}{A_k^3} \\
k_{\psi_y\psi_y} &= K_H \sum_{k=1}^{N} \frac{r_j^2 \delta_k \cos^2\phi_k (\frac{1.5 A_k ds\alpha_k^2}{\delta_k}) + A_k^2 - ds\alpha_k^2}{A_k^3}
\end{aligned}
\tag{3.39}
$$

Here the calculation of the stiffness matrix **K** is done analytically using the equations

above. This formulation expresses the dependency of the stiffness to the displacement vector u. Thus the 6 x 6 stiffness matrix $\mathbf{K}$ is formulated as so:

$$\mathbf{K} = \begin{bmatrix} K_{xx} & k_{xy} & k_{xz} & k_{x\psi_x} & k_{x\psi_y} & 0 \\ & k_{yy} & k_{yz} & k_{y\psi_x} & k_{y\psi_y} & 0 \\ & & K_{zz} & k_{z\psi_x} & k_{z\psi_y} & 0 \\ & sym. & & k_{\psi_x\psi_x} & k_{\psi_x\psi_y} & 0 \\ & & & & k_{\psi_y\psi_y} & 0 \\ & & & & & 0 \end{bmatrix} \tag{3.40}$$

In the following example, the Standard model is used. The FAG6404 ball bearing is used. In this case, a varying inner ring displacement in the axial direction u_z is applied, from 0 to 100 μm. A constant rotational speed of 3 $krpm$ is applied.

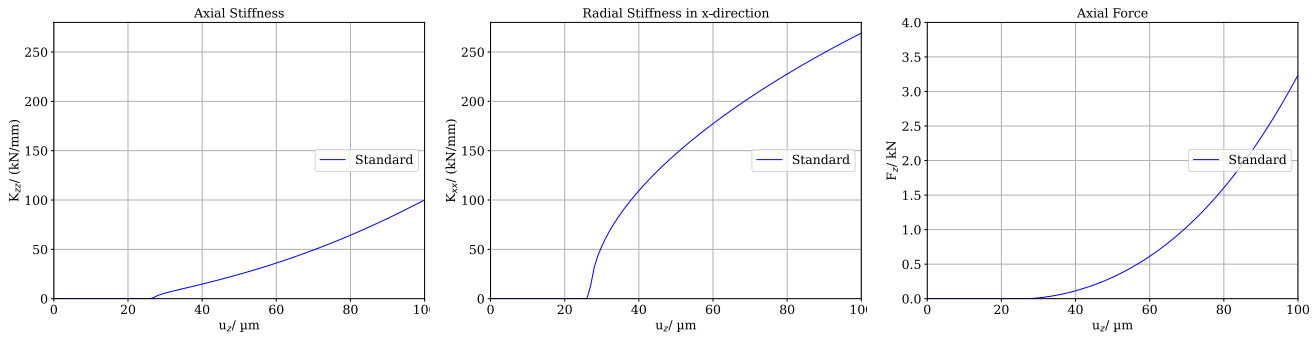

Figure 3.6: Standard Model (LS) for Varying Inner Ring Axial Displacement

It is evident that during the first steps of the displacement, no development of force or stiffness occurs. This phenomenon takes place because of the bearing's clearance, as discussed in 3.14 and 3.15. No contact occurs, hence there is no elastic deflection to produce contact reaction and Hertzian stiffness. Notice how the point of contact is identical at the bearing's stiffness, in the corresponding direction (axial,radial). This occurs because in the example above, the bearing is loaded with purely axial displacement. Thus, for the case of 3.14, it is only dependent on the bearing's geometry. As a result, the point of contact, which determines the development of force, is going to be the same for both cases, axial and radial. Additionally, it is notable that by applying a displacement, development of stiffness occurs. Not only that, but the stiffness that occurs is non-linear. Thus, there is a clear correlation between load and stiffness (load dependency of bearing).

3.2 Extended Lim and Singh Model

The following model is an extension of the standard modelling to Lim and Singh, as it uses the product of derivatives in order to calculate the force and stiffness matrices.

The derivatives are produced by deriving the elastic deformation Q_n to the inner ring displacement vector u. However, in this thesis, the Hertzian parameter that is being used is depended to the inner ring displacement. As a result the analytical expressions of the derivatives are very complex and difficult to calculate. The main goal is to determine the accuracy of the Lim and Singh simplified expressions, compared to the actual analytical expressions. As proven above, $K_{H_k} = f(\alpha_k g(u))$, hence by deriving in respect to u, we can obtain the analytical expressions of that model. That way, it is expected to have more accuracy regarding the calculations, as the different contacts are taken into consideration. In this particular example, the derivation has only been made in respect to the axial displacement u_z, for comparison reasons. The stiffness matrix $\mathbf{K}$ is produced by the general stiffness expression, as the sum of each ball's contribution:

$$K_k = \frac{\partial Qn,k}{\partial u}\mathbf{e_{f,k}} + \frac{\partial \mathbf{e_{f,k}}}{\partial u}Qn,k \tag{3.41}$$

The projection vector that is being used here is suggested by Wagner [26] as:

$$\mathbf{e}_{f,k} = \left\{ \begin{array}{c} \cos\alpha_k \cos\phi_k \\ \cos\alpha_k \sin\phi_k \\ \sin\alpha_k \\ r_j \sin\alpha_k \sin\phi_k \\ -r_j \sin\alpha_k \cos\phi_k \\ 0 \end{array} \right\} \tag{3.42}$$

For this particular example only the first three derivatives shall be used (u_x, u_y, u_z).The procedure is done as follows:

$$\frac{\partial u_r}{\partial u_z} = \cos\phi_k, \tag{3.43}$$

$$\frac{\partial u_a}{\partial u_z} = 1 \tag{3.44}$$

Then $\frac{\partial \alpha_k}{\partial(u)}$ reads as:

$$\frac{\partial \alpha_k}{\partial u_x} = \frac{\cos^2 \alpha_k}{dsr_k} \left(\frac{-ds\alpha_k \cos \phi_k}{dsr_k} \right), \tag{3.45}$$

$$\frac{\partial \alpha_k}{\partial u_y} = \frac{\cos^2 \alpha_k}{dsr_k} \left(\frac{-ds\alpha_k \sin \phi_k}{dsr_k} \right), \tag{3.46}$$

$$\frac{\partial \alpha_k}{\partial u_z} = \frac{\cos^2 \alpha_k}{dsr_k}, \tag{3.47}$$

$$\frac{\partial \alpha_k}{\partial \psi_x} = \frac{\cos^2 \alpha_k}{dsr_k} \left(r_j \sin \phi_k \right), \tag{3.48}$$

$$\frac{\partial \alpha_k}{\partial \psi_y} = \frac{\cos^2 \alpha_k}{dsr_k} \left(-r_j \cos \phi_k \right), \tag{3.49}$$

$$\frac{\partial \alpha_k}{\partial \psi_z} = 0 \tag{3.50}$$

The derivative for the local deflection δ_k is given as:

$$\frac{\partial \delta_k}{\partial u_x} = \frac{1}{2A_k} \left(2dsr_k \frac{\partial u_r}{\partial u_z} \right), \tag{3.51}$$

$$\frac{\partial \delta_k}{\partial u_y} = \frac{1}{2A_k} \left(2ds\alpha_k \frac{\partial u_a}{\partial u_z} \right), \tag{3.52}$$

$$\frac{\partial \delta_k}{\partial u_z} = \frac{1}{2A_k} \left(2dsr_k \sin \phi_k \right), \tag{3.53}$$

$$\frac{\partial \delta_k}{\partial \psi_x} = \frac{1}{2A_k} \left(2ds\alpha_k 2r_j \sin \phi_k \right), \tag{3.54}$$

$$\frac{\partial \delta_k}{\partial \psi_y} = \frac{1}{2A_k} \left(-2ds\alpha_k 2r_j \cos \phi_k \right), \tag{3.55}$$

$$\frac{\partial \delta_k}{\partial \psi_z} = 0 \tag{3.56}$$

Finally, the derivation $\frac{\partial \mathbf{e_{f,k}}}{\partial(u)}$ reads as:

$$\frac{\partial \mathbf{e_{f,k}}}{\partial u_x} = \frac{\partial \alpha_k}{\partial u_x} \cos \phi_k \left(-\sin \alpha_k \right), \tag{3.57}$$

$$\frac{\partial \mathbf{e_{f,k}}}{\partial u_y} = \frac{\partial \alpha_k}{\partial u_y} \sin \phi_k \left(-\sin \alpha_k \right), \tag{3.58}$$

$$\frac{\partial \mathbf{e_{f,k}}}{\partial u_z} = \frac{\partial \alpha_k}{\partial u_z} \cos \alpha_k, \tag{3.59}$$

Then, each Hertzian parameter from (2.14) is derived with respect to u_z accordingly. So

a K_H derivative occurs as:

$$\frac{\partial K_H}{\partial u_z} = -(K_{H,in} + K_{H,out}) \left(\frac{\frac{\frac{\partial K_{H,in}}{\partial u_z}}{K_{H,in}}^{\frac{1}{3}} + \frac{\frac{\partial K_{H,out}}{\partial u_z}}{K_{H,out}}^{\frac{1}{3}}}{(K_{H,in}^{\frac{2}{3}} + K_{H,out}^{\frac{2}{3}})^{\frac{5}{2}}} \right) \tag{3.60}$$

An example of the occurring partial derivative of $Q_{n,k}$:

$$\frac{\partial Q_{n,k}}{\partial u_z} = 0.5\sqrt{\delta_k} \left(2\delta_k \frac{\partial K_{H,k}}{\partial u_z} + 3K_{H,k} \frac{\partial \delta_k}{\partial u_z} \right) \tag{3.61}$$

Finally, the axial stiffness K_{xx} can be denoted as:

$$K_{zz} = \frac{\partial Q_{n,k}}{\partial u_z} \mathbf{e_{f,k}} + Q_{n,k} \frac{\partial \mathbf{e_{f,k}}}{\partial u_z} \tag{3.62}$$

This method has been validated by using the Central Difference method for the formulation of stiffness matrix **K** :

$$k_{i,j} = \frac{F_{max,j} - F_{min,j}}{2\Delta u} \tag{3.63}$$

,where $i \epsilon [1,6]$ and $j \epsilon [1,6]$. Essentially, for each coordinate of the stiffness matrix, the maximum and minimum force that can be generated, is calculated. Then, it is divided by an increment Δu. Using the previous example (FAG6404 bearing and varying u_z displacement), we compare the standard and the extended models.

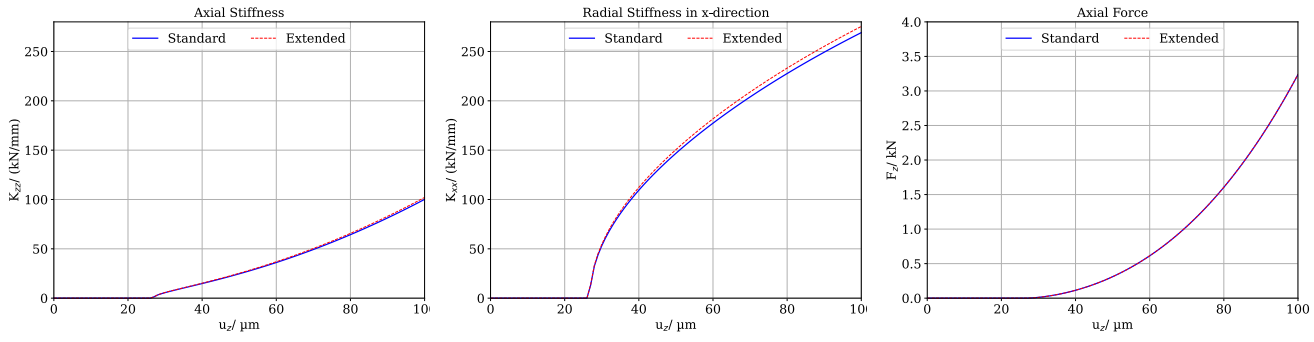

Figure 3.7: Comparison Between Standard (LS) and Extended Model with Hertzian Stiffness Coefficient Dependent on Loaded Contact Angle α_k

As it is evident from the figures above, the difference between the two methods is detrimental. In order to avoid high computational load, it is recommended to use the Standard model with the simple analytical expressions. The stiffness coefficient seem to have an almost non existent effect in the whole axial displacement operation.

3.3 Elastohydrodynamic - EHD Model

In this model, the bearing is assumed to be under lubricated conditions. Hence, to describe its behaviour the elastohydrodynamic lubrication (EHD) theory will be used. The lubrication in bearings has the purpose of reducing the friction between the rolling elements and the raceway, thus extending the wear. At this stage, it is essential to study this phenomenon, as it influences the elastic deformation, affecting the elastic force, stiffness and damping behaviour. Additionally, it is essential to model this lubrication effects that occur during the bearing operation, in order to achieve more realistic results. The following section, investigates the effects and the way to effectively model this.

3.3.1 EHD Contact Theory

When a lubricant is applied, a film between the mating surfaces of the different machine elements (rolling element, inner/outer ring etc.) forms. During operation, the fluid film experiences high pressure loads because of the mating elements, causing a series of effects such as deformations, damping behaviour, slipping etc. This phenomenon is known as elastohydrodynamic lubrication. In this section it is abbreviated as EHD. In the dry Standard model, no damping takes place, as there is no lubricant to generate the viscous damping. Material damping is neglected as it is significantly low. Hence, the damping qualities reflect the qualities of the applied lubricant. The quality of damping is also reflected in the amplitude of vibrations that the system generates. This will be further investigated in the Transient Analysis section.

The closest approach of describing this phenomenon is the Reynolds equation: This time dependent equation, contains the fluid film pressures, the geometry of the deformed gap and the velocities of the contacting surfaces. However, this thesis is not going to go in depth about the solution of this equation. Here, the effect of the EHD contact will be calculated following the suggested parameters of Wagner [26]. It is assumed that only elliptical contacts occur and that pure rolling conditions are in effect.

At this point, the speed effect is introduced into the modelling. When in high speeds, the incompressible lubricant, with a film thickness of h_0, compresses even more the mated areas, producing a different local deflection δ as before $\cdot$ the δ_{EHD}:

$$\delta = \delta_H - \delta_{EHD} \tag{3.64}$$

where δ is the total deflection that occurs and δ_H is the elastic deformation caused by Hertzian -dry- contact.

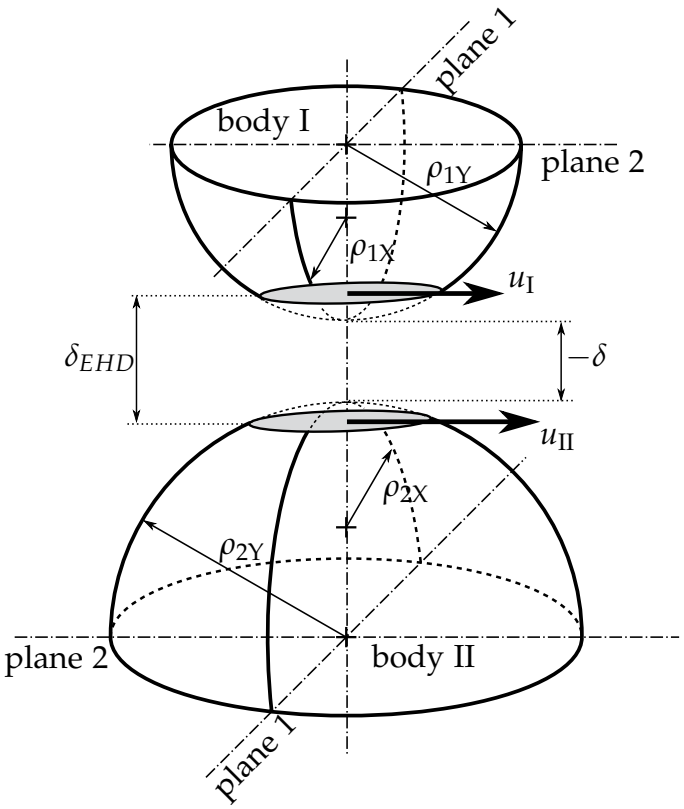

Figure 3.8: EHD Contact of Two Curved Bodies [26]

The viscous qualities of the lubricant also result in generating a viscous damping, which will also be modelled. However, in really slow speed, the effect of the lubricant is minimum, hence there is almost an identification of the dry and the lubricated contact. Concluding, in order for the EHD phenomenon to be in effect, high speed must be in effect:

$$\omega_{c,k} = \frac{\Omega}{2}\left(1 - \frac{b_r \cos\alpha_k}{p_r}\right), \tag{3.65}$$

$$\omega_{b,k} = \frac{b_r \Omega}{2b_r\left(1 - \frac{b_r \cos\alpha_k}{p_r}\right)^2}, \tag{3.66}$$

$$v_{s,k} = \omega_{c,k}\left(p_r + b_r \cos\alpha_k\right) + \omega_{b,k} b_r \tag{3.67}$$

Where $\omega_{c,k}$ is the cage speed of each ball's contribution, $\omega_{b,k}$ is the angular velocity of each ball and $v_{s,k}$ is the relative surface speed of each ball, b_r is the rolling element's diameter and p_r the pitch radius.

3.3.2 Determination of EHD Parameters

In order to determine the stiffness in an EHD contact, the elastic deformation under the effect of the film thickness must be calculated as expression 3.64. Once the deflection

expression is constructed as $\delta_{EHD} = f(Q_{el})$, it must be solved iteratively. This solution will provide the elastic resulting force Q_{el} that occurs when the model is under the influence of an elastohydrodynamic effect. This will provide us with a different stiffness than the previous models. In order to establish that, we utilize certain Hertzian parameters from section (2.1.4). The calculation of the EHD parameters is done using the Wensing approximations [28]. Therefore, the reduced dimensionless Moes parameters for circular contacts in incompressible fluids, M and L, read as:

$$L = \alpha_p E_{red} \left(\frac{\eta_0 v_s}{E_{red} R_X} \right)^{\frac{1}{4}} \quad M_{red} = \frac{1}{E_{red} R_X^2} \left(\frac{E_{red} R_X}{\eta_0 v_s} \right)^{\frac{3}{4}} \tag{3.68}$$

Where R_X and R_Y denote as:

$$R_X = \rho_{1X} + \rho_{2X} \quad R_Y = \rho_{1Y} + \rho_{2Y} \tag{3.69}$$

Then the reduced dimensionless load parameter N_{red} is expressed by Wijnant [29] as:

$$N_{red} = \left(\frac{R_X}{R_Y} \right)^{\frac{1}{2}} M_{red} \tag{3.70}$$

Wensing suggests this for the following curve-fit formula:

$$\Delta(N, L) = 1 - pN^q \tag{3.71}$$

Thus the deformation for the lubricated case δ_{EHD} is approximated as:

$$\delta_{EHD} = \delta_H \left(1 - pN^2 \right) \tag{3.72}$$

where

$$p = \left[(4 - 0.2L)^7 \, (3.5 + 0.1L)^7 \right]^{\frac{1}{7}} \tag{3.73}$$

and

$$q = \left[-\left(0.6 + 0.6(L + 3)\right)^{-\frac{1}{2}} \right]^{\frac{1}{7}} \tag{3.74}$$

Now, the elastic force Q_{el} must be calculated iteritavely for the total deflection δ:

$$\delta = \left(\frac{Q_{el}}{K_{H,in}} \right)^{\frac{2}{3}} \left[1 - p_{in} \left(N_{red,in} Q_{el} \right)^{q_{in}} \right] + \left(\frac{Q_{el}}{K_{H,out}} \right)^{\frac{2}{3}} \left[1 - p_{out} \left(N_{red,out} Q_{el} \right)^{q_{out}} \right] \tag{3.75}$$

Also, the film thickness h_0 can be calculated as:

$$h_0 = \left(\frac{Q_{el}}{K_{H,in}} \right)^{\frac{2}{3}} + \left(\frac{Q_{el}}{K_{H,out}} \right)^{\frac{2}{3}} - \delta \tag{3.76}$$

Note that for different contact angles $\alpha_{in}, \alpha_{out}$, each parameter must be calculated accordingly.

3.3.3 Damping Formulation

The Elastohydrodynamic effect, also causes a damping effect because of the lubrication. Therefore, it is also essential to calculate the damping forces Q_d and damping matrix $\mathbf{C}$ that occurs. The calculation of the EHD damping for each ball k follows as:

$$r = 0.98 - 0.017L \tag{3.77}$$

$$s = -0.83 - 0.008L \tag{3.78}$$

Then the elliptical half axis of the contact between the rings and the balls must be calculated. α is the elliptical half axis of the direction of motion and b the elliptical half axis of the transverse direction. These are calculated for each inner and outer contact.

$$a = \xi \left(\frac{3E_{red}}{R} \right)^{\frac{1}{3}} \tag{3.79}$$

$$b = \eta \left(\frac{3E_{red}}{R} \right)^{\frac{1}{3}} \tag{3.80}$$

Physical (dimensional) damping denotes as:

$$c = rN^s \left(\frac{4Q_{el}R}{av_s} \right) \left(\frac{\mathcal{E}}{\mathcal{K}} \right) \tag{3.81}$$

Calculated for both contacts. The total damping coefficient follows as:

$$c_{tot} = \frac{1}{\frac{1}{c_{in}} + \frac{1}{c_{out}}} \tag{3.82}$$

Therefore, the damping forces Q_d are calculated as:

$$Q_{d,k} = \dot{\delta_k} c_{tot} \tag{3.83}$$

For each ball's contribution k to the damping follows as:

$$\mathbf{C_k} = \frac{\partial \dot{\delta_k}}{\partial \dot{u}} \mathbf{e_{f,k}} c_{tot} \tag{3.84}$$

,where the partial derivation $\frac{\partial \dot{\delta_k}}{\partial \dot{u}}$ follows as:

$$\frac{\partial \dot{\delta_k}}{\partial u_x} = \frac{1}{2A_k} \left(2dsr_k \cos\phi_k\right), \tag{3.85}$$

$$\frac{\partial \dot{\delta_k}}{\partial u_y} = \frac{1}{2A_k} \left(2dsr_k \sin\phi_k\right), \tag{3.86}$$

$$\frac{\partial \dot{\delta_k}}{\partial u_z} = \frac{1}{2A_k} \left(2ds\alpha_k\right), \tag{3.87}$$

$$\frac{\partial \dot{\delta_k}}{\partial \psi_x} = \frac{1}{2A_k} \left(2ds\alpha_k r_j \sin\phi_k\right), \tag{3.88}$$

$$\frac{\partial \dot{\delta_k}}{\partial \psi_y} = \frac{1}{2A_k} \left(-2ds\alpha_k r_j \cos\phi_k\right), \tag{3.89}$$

$$\frac{\partial \dot{\delta_k}}{\partial \psi_z} = 0 \tag{3.90}$$

The previous expressions can be used to obtain the damping forces $F_{d,k}$:

$$F_{d,k} = Q_{d,k}\mathbf{e_{f,k}} \tag{3.91}$$

Finally, the damping matrix $\mathbf{C}$ is the sum of each ball's contribution:

$$\mathbf{C} = \begin{bmatrix} c_{xx} & c_{xy} & c_{xz} & c_{x\psi_x} & c_{x\psi_y} & 0 \\ & c_{yy} & c_{yz} & c_{y\psi_x} & c_{y\psi_y} & 0 \\ & & c_{zz} & c_{z\psi_x} & c_{z\psi_y} & 0 \\ & sym. & & c_{\psi_x\psi_x} & c_{\psi_x\psi_y} & 0 \\ & & & & c_{\psi_y\psi_y} & 0 \\ & & & & & 0 \end{bmatrix} \tag{3.92}$$

Although, damping is produced, the damping forces Q_d are kept very low. As it is shown in the figure 3.9 the damping, while it is indeed kept low, it is also non-linear to the displacement. This non-linearity is worth mentioning, however the values are so low that the damping provided is not sufficient for the following transient analysis. Thus, in later investigation of the transient analysis, a proportionate damping is used instead of the bearing's damping, in order to be able to produce realistic results. It also must be noted that the EHD model returns both inner ring elastic forces F and damping forces F_d.

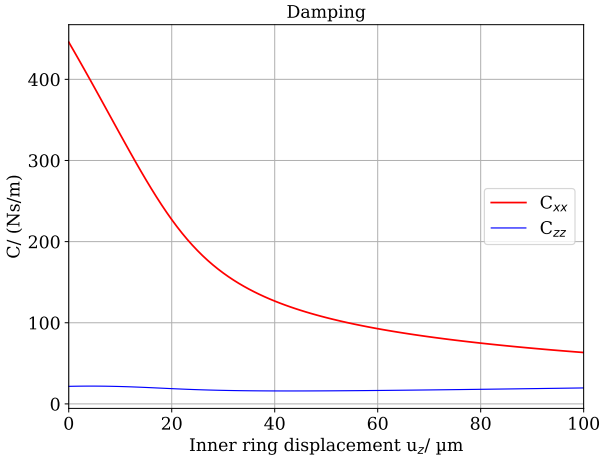

Figure 3.9: EHD Damping in Radial C_{xx} and Axial C_{zz} Direction to Inner Ring Axial Displacement

3.4 Model Comparison

The purpose of the following chapter is to make a distinction between the different kinematic models, on a larger scale. This investigation allows to see the different effects that each addition in the modelling have in the resulted force and stiffness.

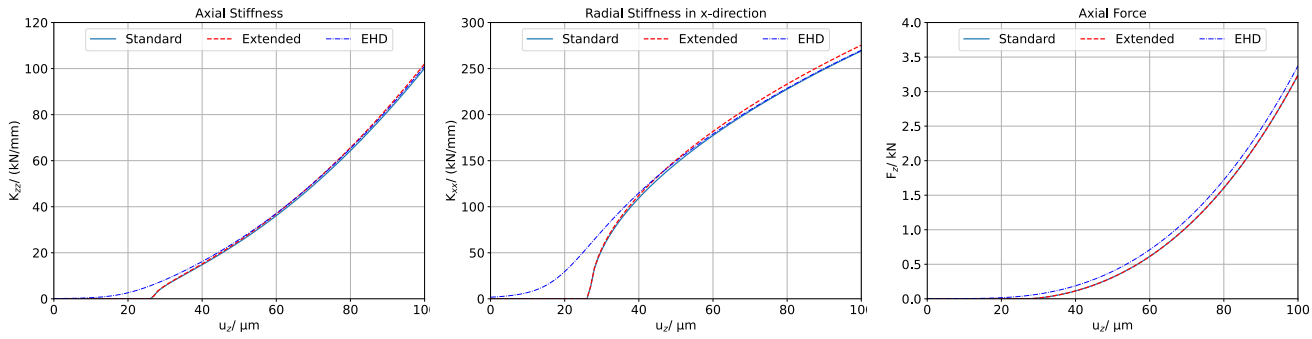

Figure 3.10: Comparison Between Standard (LS), Extended (K_H Dependency on α_k) and EHD Model

It is quite evident that there is little to no difference between the Standard and Extended models. Thus, we confirm that the LS formulations of force and stiffness are quite accurate. Also, it is derived that little to no difference occurs when there is a varying Hertzian parameter K_H in the model. However, for general accuracy reasons a varying K_H will be used for further modelling. In the Standard and Extended model, a free play occurs, in both axial and radial direction. This is due to the clearance bounds, as it was touched on 3.14 and 3.15. In the case of EHD, little to no free play is resulted, as the contact is almost immediate because of the lubricant. Thus, force and stiffness develop in faster in terms of displacement, compared to the other two models.

4 Dynamic modelling

The purpose of this chapter is to introduce the dynamic modelling into the simulation. In this case, the Dynamic equilibrium is used. This includes the forces of the balls, all the acting forces, centrifugal force and moments. This modelling is referred to as "Full Model" and it consists all of the above phenomena that have been previously discussed such as: Additional degrees of freedom of the ball, varying Hertzian parameter K_H, EHD contact and solving the dynamic equilibrium. Furthermore, a new formulation of kinematics is introduced and compared to.

4.1 Full Model

The Full implementation takes into account the additional ball Degrees of Freedom (DoFs) to provide a more accurate representation of the bearing's actual behaviour. In order to establish that, the ball DoFs (u_{br},u_{ba}) are calculated iteratively. Furthermore, the Full model takes into consideration the centrifugal force F_z and gyroscopic moment M_g which will be mentioned later on.

4.1.1 Full Model Formulation

Firstly, this model takes an input of u_b 2N ball degrees of freedom, where N is the number of balls:

$$u_b = [u_{ba} \;\; u_{br} \;\; \dot{u_{ba}} \;\; \dot{u_{br}}] \tag{4.1}$$

where α and r, axial and radial direction respectively.

By initializing this vector, we proceed by solving iteratively the following dynamic equilibrium. This way we obtain the degrees of freedom to proceed and calculate the produced forces $\mathbb{F}$ of the inner ring:

$$m_b \ddot{u_{ba}} = (Q_{n,in} + Q_{d,in}) \sin \alpha_{in} + Q_{t,in} \cos \alpha_{in} - (Q_{n,out} + Q_{d,out}) \sin \alpha_{out} - Q_{t,out} \cos \alpha_{out} \tag{4.2}$$

$$m_b \ddot{u_{br}} = (Q_{n,in} + Q_{d,in}) \cos \alpha_{in} - Q_{t,in} \sin \alpha_{in} - (Q_{n,out} + Q_{d,out}) \cos \alpha_{out} + Q_{t,out} \cos \alpha_{out} + Fz \tag{4.3}$$

where *mb* is the rolling elements mass and denotes as:

$$m_b = \rho \left(\frac{4}{3} \pi r_b^3 \right) \tag{4.4}$$

where ρ is the density of the ball's material.

Since this model includes additional degrees of freedom, new kinematic formulations are introduced, as suggested by Wagner [26]:

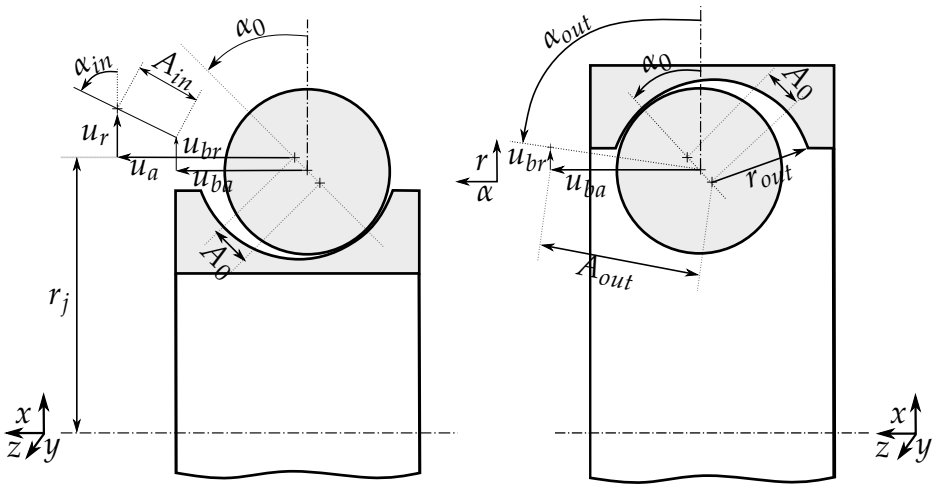

Figure 4.1: Additional Kinematics as Suggested by Wagner [26]

This set of kinematics is used when the bearing is preloaded, so it doesn't take into account the radial displacement r_L. Because of the additional degrees of freedom, the contact angles are formulated differently:

For inner ring contact:

$$ds\alpha_{in} = u_\alpha - u_{ba} + 0.5 A_0 \sin \alpha_0, \tag{4.5}$$

$$dsr_{in} = u_r - u_{br} + 0.5 A_0 \cos \alpha_0 \tag{4.6}$$

$$A_{in} = \sqrt{ds\alpha_{in}{}^2 + dsr_{in}{}^2} \tag{4.7}$$

$$\alpha_{in} = \arctan \left(\frac{ds\alpha_{in}}{dsr_{in}} \right) \tag{4.8}$$

and the theoretical elastic deformation of the inner ring denotes as:

$$\delta_{in} = \begin{cases} A_{in} - 0.5 A_0, & (A_{in} - 0.5 A_0) > 0 \\ 0, & (A_{in} - 0.5 A_0) \leq 0 \end{cases} \tag{4.9}$$

Similarly, for outer ring contact:

$$ds\alpha_{out} = u_{ba} + 0.5A_0 \sin\alpha_0, \tag{4.10}$$

$$dsr_{out} = u_{br} + 0.5A_0 \cos\alpha_0 \tag{4.11}$$

$$A_{out} = \sqrt{ds\alpha_{out}{}^2 + dsr_{out}{}^2} \tag{4.12}$$

$$\alpha_{out} = \arctan\left(\frac{ds\alpha_{out}}{dsr_{out}}\right) \tag{4.13}$$

and the theoretical elastic deformation of the outer ring is expressed as:

$$\delta_{out} = \begin{cases} A_{out} - 0.5A_0, & (A_{out} - 0.5A_0) > 0 \\ 0, & (A_{out} - 0.5A_0) \leq 0 \end{cases} \tag{4.14}$$

Upon further investigation on the kinematics, a new formulation occurred. While the above kinematics use a loaded geometry, it would be more optimal to take into consideration the position of the bearing when it is unloaded. An investigation between both formulations will take place. In order to make a distinction, the new formulation will be referred to as " updated ".

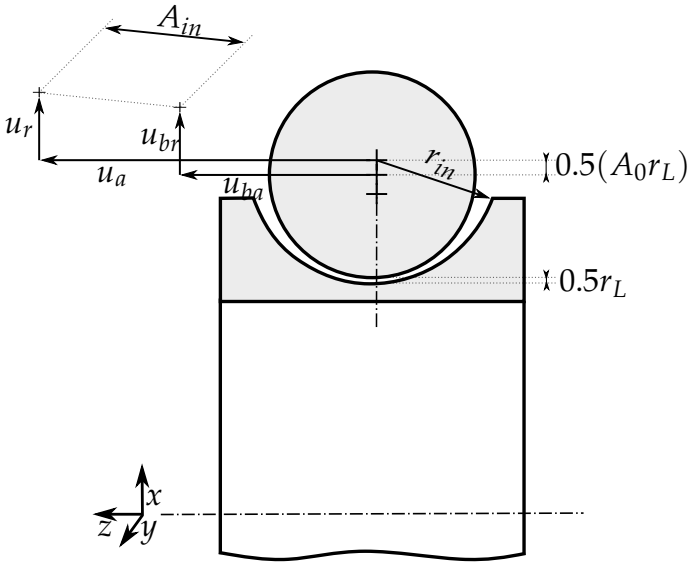

Figure 4.2: Updated Kinematics

The new updated formulations denote as so:

For inner ring contact the new expressions are:

$$ds\alpha_{in} = u_{\alpha} - u_{ba}, \tag{4.15}$$

$$dsr_{in} = u_r - u_{br} + 0.5\,(A_0 - r_L) \tag{4.16}$$

$$A_{in} = \sqrt{ds\alpha_{in}{}^2 + dsr_{in}{}^2} \tag{4.17}$$

$$\alpha_{in} = \arctan\left(\frac{ds\alpha_{in}}{dsr_{in}}\right) \tag{4.18}$$

and the theoretical elastic deformation of the inner ring denotes as:

$$\delta_{in} = \begin{cases} A_{in} - 0.5A_0, & (A_{in} - 0.5A_0) > 0 \\ 0, & (A_{in} - 0.5A_0) \leq 0 \end{cases} \tag{4.19}$$

Similarly, the updated expressions for outer ring contact:

$$ds\alpha_{out} = u_{ba}, \tag{4.20}$$

$$dsr_{out} = u_{br} + 0.5\,(A_0 - r_L) \tag{4.21}$$

$$A_{out} = \sqrt{ds\alpha_{out}{}^2 + dsr_{out}{}^2} \tag{4.22}$$

$$\alpha_{out} = \arctan\left(\frac{ds\alpha_{out}}{dsr_{out}}\right) \tag{4.23}$$

and the theoretical elastic deformation of the outer ring is expressed as:

$$\delta_{out} = \begin{cases} A_{out} - 0.5A_0, & (A_{out} - 0.5A_0) > 0 \\ 0, & (A_{out} - 0.5A_0) \leq 0 \end{cases} \tag{4.24}$$

It must be highlighted that with the above change, the force free axial and radial movement lead to be equal to the axial and radial clearance, accordingly. This is due to the new state of the ball position, as it now lays in a centred position. As a result, the representation of a realistic force free movement of the inner ring renders possible.

As discussed above, the Full model includes the EHD effect. Thus in this model the calculation of the elastic force Q_{el} takes place. The normal, tangential and damping forces are also added into the equilibrium (Q_n, Q_t, Q_d) Additionally, the centrifugal and gyroscopic phenomena are added. These are discussed in detail further on with the explanation of the race control. It must be noted that there is a distinction between the lubricated and non-lubricated full model. This will be mentioned again on the ADORE validation examples. When the user chooses the non-lubricated case, then $Q_{el} = Q_n$ and the EHD module is deactivated. This makes the calculations a lot faster, as we skip the iteration.

4.2 Race Control Hypothesis

In order to achieve a better comparison to ADORE [8], some parameter investigation was done. A correlation between the ball pitch angle a_b and the race control was . According to Harris [11], a ball pitch angle is referred to as the angle between the vector of the ball's angular velocity vector around it's centre and x-axis. The angular velocity vector, is expressed through two types of other components: the rolling motion and the spinning motion of the ball. Thus the ball pitch angle, expresses the rolling and spinning motions that occur to the rolling elements during operations. To be more specific, in ball bearings with non zero contact angles between the rolling elements and raceways with high-speed applications, motions like sliding, spinning and gyroscopic motions occur. In order to differentiate the motions that will be addressed later on, a description of each phenomena will be made.

4.2.1 Rolling, Spinning and Sliding Motion

A rolling element of the ball bearing, moves in respect to the raceway, about the generatrix of motion. The generatrix of motion may be intersected with the contact line at a singular point, thus In the following applications, a pure rolling condition is assumed. Pure rolling between two contacting surfaces can be obtained when:

- Mathematical line contact under zero load
- Line contact in which the contact bodies are identical in length
- Mathematical point contact under zero load

However, when the spinning vector component acts normal to the surface, it causes a spinning effect, around the pure rolling point. This combination of spin and rolling of the ball, creates a contact ellipse that the ball operates on, in contact with the inner and outer race respectively. This phenomenon that occurs is called sliding motion. This sliding motion, is caused by the gyroscopic moment that occurs to each loaded ball, when the contact angle α_k is non zero.

4.2.2 Race Control Dependency

Depending on the distribution of the moment between the inner and the outer ring, the dynamic equilibrium changes. As a result, different ball bearing displacements (u_{ba},u_{br}) are returned by the solver. Consequently, producing different stiffnesses, as they are calculated numerically, using the returned u_{ba},u_{br}. It must be noted that the stiffness is calculated numerically by using the Central Difference method 3.63.

This distribution of transfer is controlled via race control. Generally, when pure rolling occurs, there is also a spinning motion happening, either at the inner or outer race contacts. That is for non zero contact angles. When the race control is in effect in either

race, it indicates that no spin occurs at said race contact. Hence the ball is controlled by that race. To be more specific, a pure rolling motion is obtained between the ball and the race that has the control at the moment. To express what type of control is in effect, a λ parameter is introduced. This parameter controls the transfer of the gyroscopic moment between the contacts. According to Servais [23], for λ equal to zero, inner race control is in effect, whereas for λ equal to one, outer race control is established. According to the configuration, the ball pitch angle of the ball, interchanges between the α_{out} and α_{in}. Similarly, when $\lambda = 0$, $\alpha_b = \alpha_{in}$. Additionally, when full race control occurs on one of each races, it suggests that the all the tangential forces Q_t effect is produced by said race contact. However, this is not fully representative of the real interchange of the ω_b plane and the distribution of the tangential forces Q_t between the races. Consequently, the dynamic equilibrium changes. After establishing that indeed there is an implicit connection between the transfer percentage of the gyroscopic moment and the stiffness, a formula was developed to take this into consideration.

The main notion of the formula is to determine a parameter λ, where $0 \leq \lambda \leq 1$ that represents the race control that is in effect. In order to make the formula more robust the following expression was followed:

$$\lambda_{out} = \frac{\frac{1}{Q_{n,out}} + \frac{1}{Q_{n,in}}}{Q_{n,in}} \tag{4.25}$$

$$\lambda_{in} = 1 - \lambda_{out} \tag{4.26}$$

The notion behind this is formula is, the race that carries the most normal forces, has a better contact, hence is more unlikely to have slip. In order to prove that, the following expression from Wagner [26], for dry pure Hertzian contact was taken:

$$\frac{Q_{t,in}}{Q_{t,out}} = \frac{Q_{n,in}}{Q_{n,out}} \Rightarrow \frac{Q_{t,in}}{Q_{t,out}} = \frac{1-\lambda_{out}}{\lambda_{out}} \Rightarrow \frac{Q_{n,out}}{Q_{n,in}} = \frac{1-\lambda_{out}}{\lambda_{out}} \Rightarrow \lambda_{out} = \frac{\frac{1}{Q_{n,out}} + \frac{1}{Q_{n,in}}}{Q_{n,in}} \tag{4.27}$$

This formulation works for dry contact. In order to handle the lubricated case or make it even more accurate in regards of load distribution, it is suggested to investigate the ellipse's contact velocities given by Jones [12] as Servais [24] suggests.

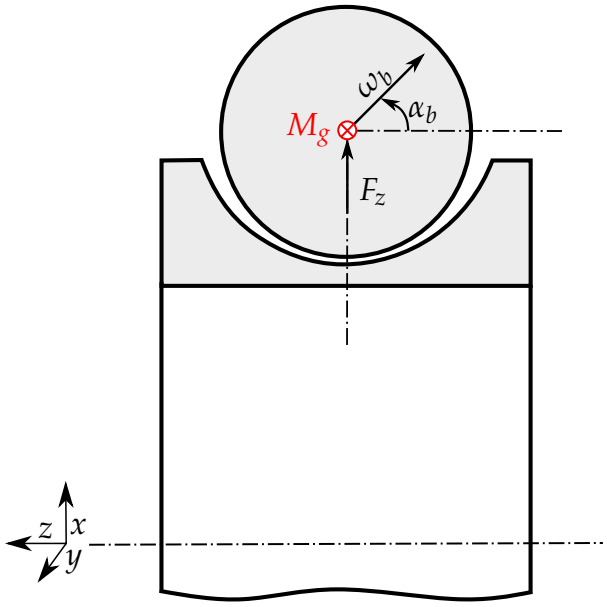

Figure 4.3: Ball Pitch Angle α_b, Centrifugal Force F_z and Gyroscopic Moment M_g

This statement indicates the amount of normal forces that are applied to each ring contact accordingly. For example, when the contact is greater on the outer ring, then the normal forces increase in that point of contact. Thus, the amount of friction that is generated there is larger, compared to the inner ring. For a large amount of friction, the slip decreases. In this case, the race that is in control is the outer one. Similarly, when the inner ring is accountable for the larger percentage of friction, then inner race is in control. Hence, having in effect the λ for the calculation of the tangential forces, would benefit in a more accurate representation of the transferable friction percentage to each ring. The tangential forces are then given as:

$$Q_{t,in} = \frac{2M_g}{D_b}(1 - \lambda_{out}) \quad Q_{t,out} = \frac{2M_g}{D_b}\lambda_{out} \tag{4.28}$$

,where M_g is the gyroscopic moment and J_b the moment of inertia of the ball:

$$J_b = 0.4 m_b b_r^2 2 \tag{4.29}$$

$$M_g = J_b \omega_b \omega_c \sin\alpha_b \tag{4.30}$$

The ball pitch angle α_b is expressed here as:

$$\alpha_b = \alpha_{in}(1 - \lambda_{out}) + \alpha_{out}\lambda_{out} \tag{4.31}$$

To showcase the sensitivity due to race control, the following example uses the FAG6404 and the Full dry model, with updated kinematics. We have a constant axial force of 5 kN and rotational speed Ω that varies from 0 to 60 $krpm$.

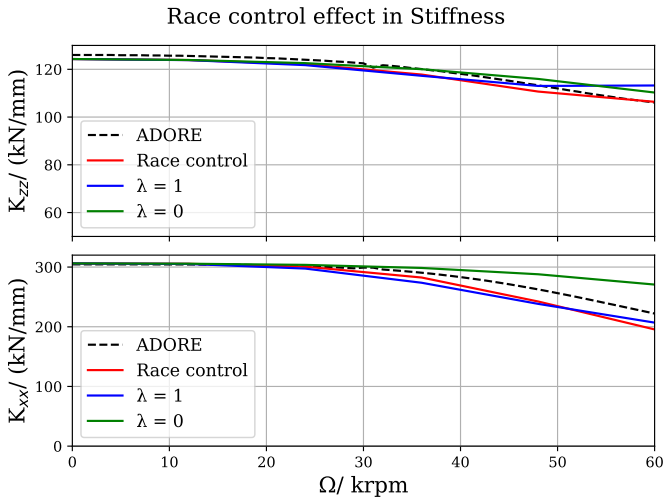

Figure 4.4: Stiffness Dependency of Race Control Hypothesis: $\lambda = 1$ (Outer Race Control), $\lambda = 0$ (Inner Race Control) and ADORE

As it is shown above, the modelling is very sensitive to the configuration of the λ. For outer race control, the model underestimates the ADORE results for the axial stiffness K_{xx}, whereas the radial stiffness K_{zz} is overestimated. For inner race control, the results are even further to the ADORE calculation. Regarding the feedback race control, a better approach to K_{xx} is achieved. However, in regards of K_{zz}, a deviation occurs. This is due to the λ implementation in the equilibrium loop. In conclusion, it is highly likely that the tangential forces Q_t are sensitive to this λ factor, heavily influencing the dynamic equilibrium calculation.

4.2.3 Ball Pitch Angle Dependency

Keeping the race control hypothesis in effect, the ball pitch angle can now be investigated. The ball pitch angle α_b 4.3, indicates the position of the ball rotational axis ω_b, on the specific plane of rotation. This angle is used for the calculation of the gyroscopic moment M_g. Different approaches of this angle, changes the behaviour of the whole bearing. This is due to the implicit connection this angle has with the dynamic equilibrium. Three different expressions were investigated: a_b is given above 4.31, θ is expressed by Kurvinen [15] and b by Wang [27]. Using the same example as 4.4, we sustain the race control hypothesis, and change the different ball pitch angle configurations.

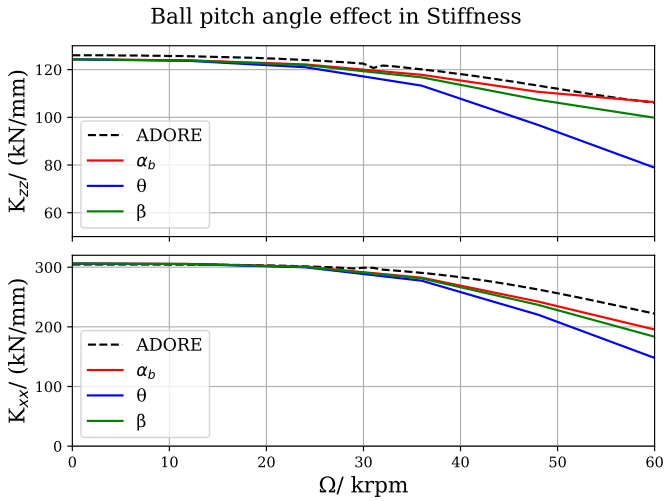

Figure 4.5: Different Ball Pitch Angle Configurations and their Effect on the Bearing's Stiffness

It is evident that in this case, the best case is the α_b configuration, which will be used for the rest of the thesis. However, it is notable that Noel[21] and Antoine[1] have made suggestions on how to approximate more accurately the ball pitch angle, by doing various iterations. While this is an interesting topic, it is not the specific scope of the analysis. In addition, this iteration requires more computational power and will affect the total calculation time of the modelling.

5 Validating with ADORE

ADORE is an advanced interface, that performs real time simulations of the dynamic behaviour of the rolling bearings. ADORE, operates under classical differential equations of motion and the analytical models for the interaction between the various bearing elements. A six DoF system is used to formulate the kinematic equations. ADORE is a very powerful tool that it is widely spread amongst the rotordynamic field. However, it has a complex interface for the user, in addition of being time consuming to produce certain results. In this section the data taken from ADORE, will be compared with the non-linear ball bearing models. The goal here is to investigate if similar results can be achieved with the suggested models, in an optimum amount of time, while being user friendly.

5.0.1 Standard Model Validation

It has to be taken into consideration that the following Standard model operates under dry friction conditions. Thus, the calculation of the contact area will be under a dry point contact. To establish the validation with ADORE, the FAG6404 bearing is used 8.3.1. In order to investigate the load dependency of the basic kinematic model, the rotational speed is kept at a constant 3 $krpm$ and the axial force F_z varies from 0 to 4 kN.

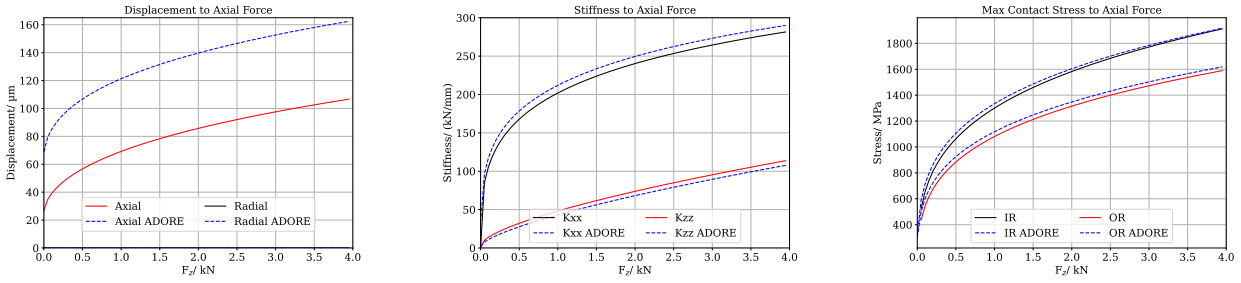

Figure 5.1: Validating with ADORE - Load Dependency of Force Stiffness and Contact Stress, using Standard (LS) Model

From the comparison of the displacement, assuming that ADORE returns the optimal solution, it seems that there is quite a relevant error between the Standard and ADORE. This can be explained from the fact that there is a difference between the kinematic formulations. ADORE uses kinematic expressions that are not accessible. Thus, this affects the displacement. As a result, stiffness (axial stiffness: K_{zz}, radial stiffness K_{xx}) and maximum stress P_{max} is affected, as they are implicitly dependent on the axial displacement u_z of the inner ring. In addition, this example showcases the non-linearity of stiffness. With the change of axial force F_z, different stiffness and force occurs (force dependency).

5.0.2 Full Model Validation

For the following validation, data from the interface ADORE has been extracted and used for comparison reasons. It is important to note once more, that the ADORE uses different kinematics, and slight difference in results is to be expected. For this example, "Dry Full" model variations will be used. That is because the race control is not fit for the lubricated case, as it considers only dry contact conditions. Thus, it is expected to have some variance from ADORE, as it is assumed that different lubrication configurations. Another note is that it is not clear if ADORE uses any race control hypothesis at all, or by default uses an outer race control, which is usually the case for high speed applications. A comparison between the updated and not kinematic formulations will take place, again with the FAG6404 bearing. The first example tests the load dependency of the models, with varying axial force F_z from 0 to 4 kN and a constant rotational speed of 3 $krpm$.

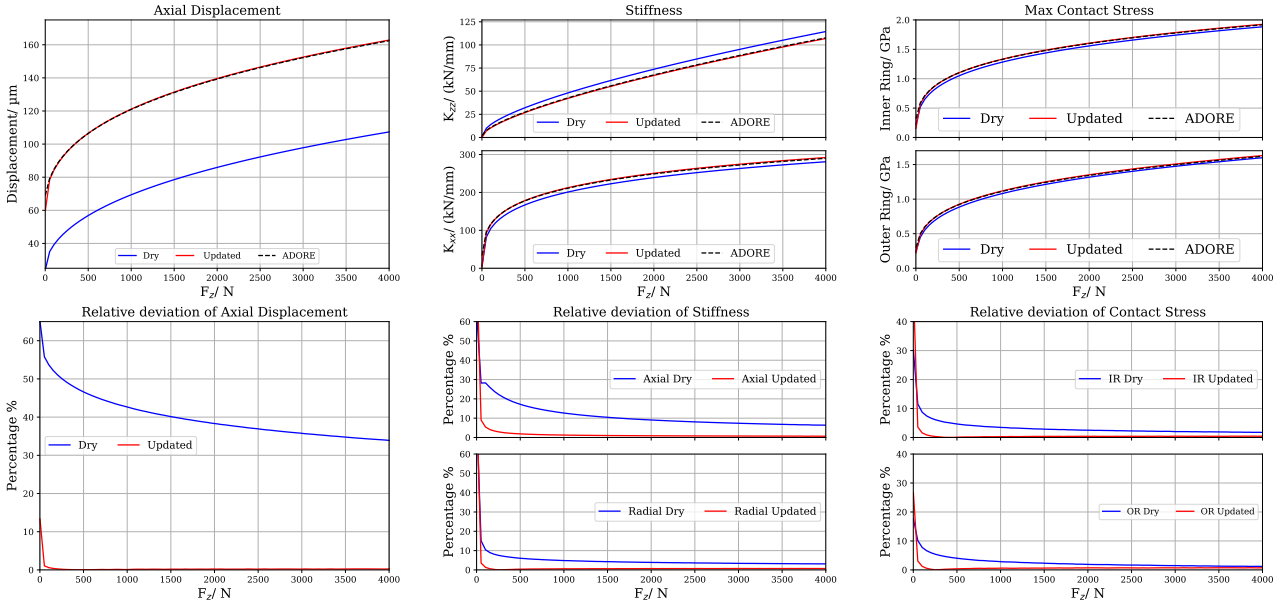

Figure 5.2: Load Dependency of Inner Ring Displacement, Stiffness and Contact Stress of Dry Full and Dry Full Updated Models and ADORE

Unquestionably, the updated kinematics have a minimal relevant error to ADORE, which has an effect on the stiffness (axial stiffness: K_{zz}, radial stiffness K_{xx}) and the stress P_{max} approximation. From the relative deviation, considering that the ADORE data is the optimum solution, the updated kinematics model establishes almost zero percent error. That carries through both in the stiffness and maximum contact stress. This proves that with improving the kinematics, we achieve less variance to ADORE. Furthermore, the load dependency of the model is evident. The second example, tests the speed dependency of the models. This time, keeping the axial force F_z constant at 5 kN and changing the rotational speed at 0 to 60 $krpm$.

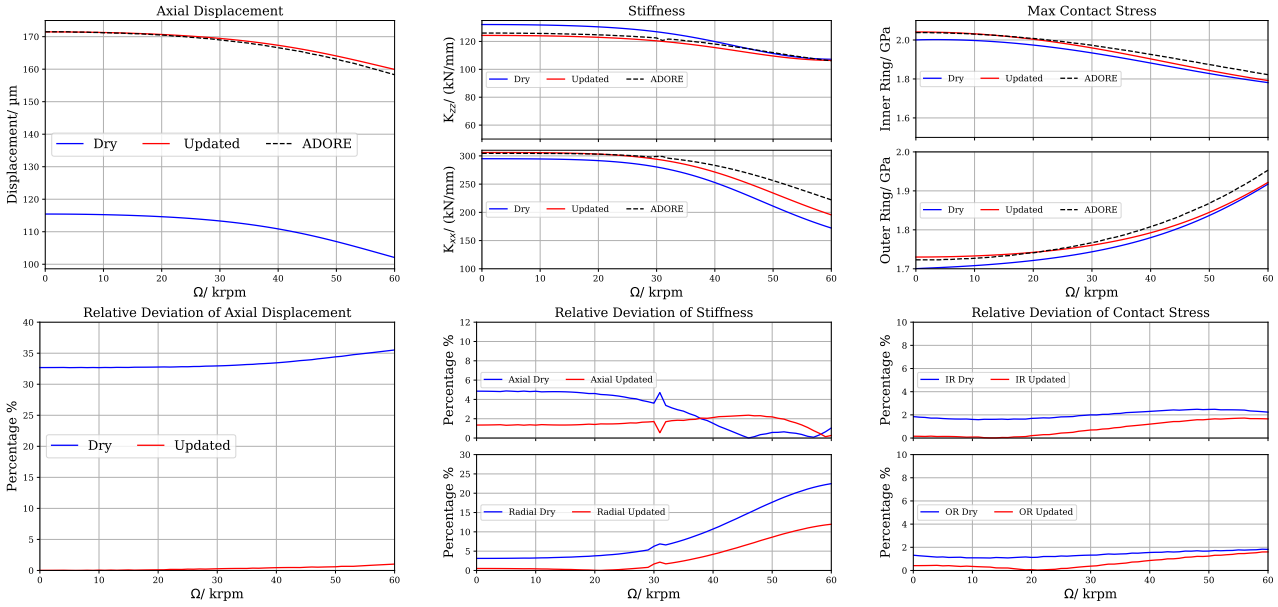

Figure 5.3: Speed Dependency of Inner Ring Displacement, Stiffness and Contact Stress of Dry Full and Dry Full Updated Models and ADORE

5.0.3 Realistic Example Using Aircraft Engine Bearing

In this chapter we test even further the capabilities of the models. Here the models are put under realistic aircraft engine operation. The models' stiffness speed and load dependency will be tested under the range of rotational speed 0 to 22.5 $krpm$, with constant thrust load of 25 KN. Furthermore, different race control scenarios will be tested, in order to establish which scenario achieves the least deviation with the ADORE data (assuming that ADORE is the optimum in each case). The model that it is used for the following example is the dynamic Full model with dry contact and updated kinematics ("Full Dry Updated" model):

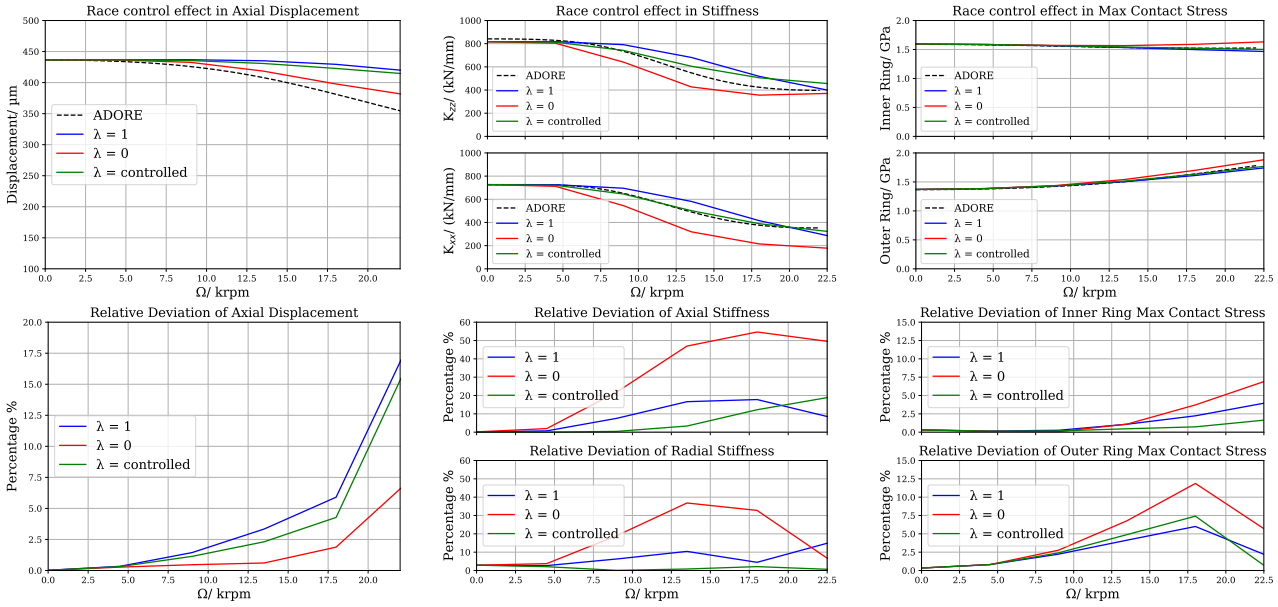

Figure 5.4: Realistic Jet Engine Bearing Operation: Influence of Race Control Compared to ADORE

First of all, it is evident that the non-linearity in stiffness and force is established due to the rotational speed. Regarding the race control configurations, it is evident that both outer and inner race control (where inner race control is $\lambda = 0$ and outer $\lambda = 1$) are over estimating the displacement. The controlled case (4.26,4.25) achieves the best approximation to ADORE, with a less than 7.5% error. Regarding the stiffness, the controlled case, lands between the outer and inner configurations. It is evident that the controlled case approaches ADORE with minimum error in the radial stiffness K_{xx}. However, in the case of axial stiffness K_{zz}, even though the controlled case is the best, the deviation still runs quite high (10 to 20%). This is expected due to the deviation in the axial inner ring displacement u_z and it is most probably due to difference in the kinematic expressions. In the calculation for the maximum stress P_{max}, all race control configurations have a low error for both outer and inner ring contact stress. The controlled case, remains as the optimal option as it maintains a very low error in outer and inner contact, even though outer race control establishes less deviation for outer race contact stress. This can be explained due to the fact that in the case for outer stress the outer control diminishes the slip effect on the outer race. Thus having a better contact and less power loss. In conclusion, race control configuration effects greatly the dynamic equilibrium due to the different force distribution that can be achieved through it. In order to achieve better results for future jet applications even for lubricated cases, the race control expression must be further investigated and reformed.

6 Rotor Coupling

In this section, the influence of the non-linear bearing on the transient response when coupled with a jet engine will be investigated. Jet engine rotors, are operating on high speeds and thrust loads. The bearings supporting the rotor, must be able to handle these high thrust loads. The goal with these non-linear bearings is to essentially have a feedback on the displacement of the rotor (load dependency), in order to produce the appropriate stiffness to support such loads. Therefore, a transient analysis is needed, to clearly see what amplitudes and resonances occur. For comparison reasons, a transient analysis with linear bearings is also done.

The coupling is achieved as so. First, to achieve the speed dependency, the rotor's rotational speed is inserted to the modelling through ϕ_0 (3.5). The exact implementation is discussed on the next section. The load dependency is achieved by matching the shaft's displacements to the inner ring's displacement vector u. This is not exactly accurate, because the inner ring's position to the shaft's is not identical. This is mostly due to the fit. However, the difference is negligible. When coupled with a certain model, the model returns the bearing forces that are being produced with the given configurations. These bearing forces will be referred as F_b for the rest of the chapter.

Influence of Cage's Circumferential Position

As it was mentioned above, to achieve the speed dependency, the rotor's speed was implemented in ϕ 3.5. Thus ia necessary to investigate the influence of the cage's circumferential position ϕ 3.5. In order to do that, the initial position of the balls ϕ_0 was manipulated accordingly. In this particular example, the displacement u_x is varying, as an input. The first case, ϕ_0 is taking values from 0° to 360°. Because of the pre-tension on the radial x direction, we see that the force F_x is fluctuating around a non-zero value. Alternatively, F_y fluctuates around zero. Both forces showcase a periodic wave for a period of 60°. This is expected, as ϕ is dependent on the terms $\frac{2\pi}{N}k$ and the number of balls in this example is equal to 6. In the second case, the same input is kept, however the initial position of the ball ϕ_0 is dependent on θ, where $\theta\epsilon[0, 360]$. θ expresses the circumferential position of the inner ring. In order to couple θ to ϕ, the geometric relation between the inner ring and the ball was used, as given from Krämer [14]:

$$\phi_0 = \frac{R_{in}}{R_{in} + R_{out}}\theta \tag{6.1}$$

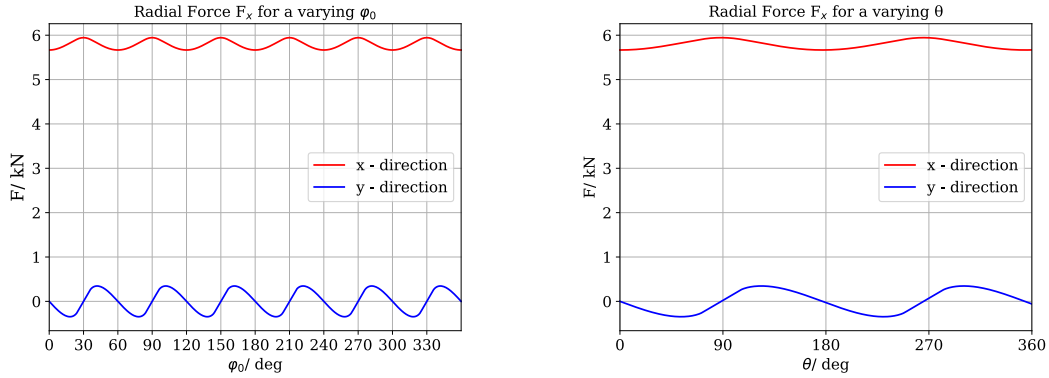

Figure 6.1: Comparison of Different Cage Configurations: $\theta \epsilon [0, 360]$ and $\phi_0 = f(\theta)$

It is evident here that the period of the wave has increased to 90°, as the initial position of the ball is proportional to the inner ring position. Thus, in order to make the overall coupling with the rotor more realistic, expression 6.1 is used. The rotor's angular position is set as equal to θ, establishing the speed dependency of the model, as realistically as possible. It has to be noted here, that the angular position of the rotor is not exactly the same as the inner ring's, due to fitting and friction. However, the error between them is negligible.

6.0.1 4 - DoF Jeffcott Rotor Example

The first coupling is done with a simple 4 DoF Jeffcott Rotor. This Jeffcott rotor model is supported by two bearings, one on each end. One unbalance is located in the middle, as seen in figure 6.2. It consists of 4 Finite Elements and each node carries 4 degrees of freedom (DoFs). Our modelling consists of 6 DoFs. However this is not a concern, we can simply set the additional degrees of freedom as constant. Of course for the coupling to work, a pre-tension needs to be added. This pre-tension can be either given by the manufacturer or a good baseline is to use the free-play calculation (3.14). The rotor is symmetrical. System stiffness **K**, mass **M** and damping **C** are given, when coupled with linear bearings. Then, the transient analysis is done by solving the time domain equation:

$$\mathbf{M}\ddot{\vec{x}} + (\mathbf{C} + \mathbf{G}(\Omega))\dot{\vec{x}} + \mathbf{K} = F + F_b \Rightarrow \ddot{\vec{x}} + \mathbf{M}^{-1}(\mathbf{C} + \mathbf{G}(\Omega))\dot{\vec{x}} = \mathbf{M}^{-1}(F + F_b) \tag{6.2}$$

This is done using the "*solveivp*" function in Python. It is suggested using the "*Radau*" or the "*BDF*" method for a fast calculation.

In regards of the system's damping **C**, Rayleigh damping is used, in order not to interfere with any additional structural damping [6]. In general, the damping that is being generated by the non-linear bearings, is not enough to support the load that is produced by the rotors. Therefore, Rayleigh damping is implemented, proportionate to the system's stiffness and mass:

$$\mathbf{C} = \alpha\mathbf{M} + b\mathbf{K} \tag{6.3}$$

where α and b are parameters defined by the user. For this particular example an α equal to 0.5 and b of $1e-4$ was used.

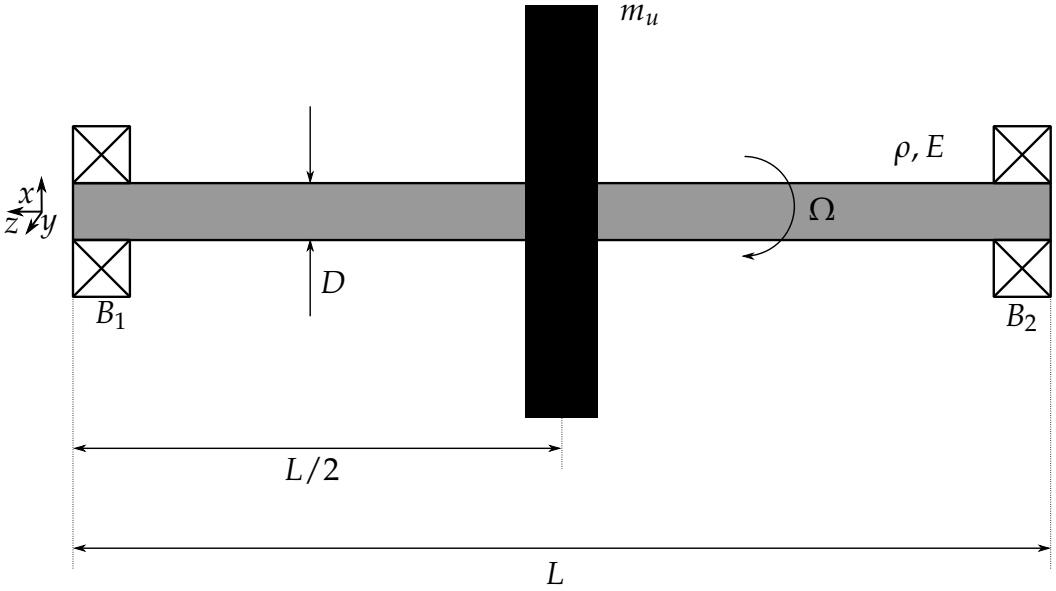

Figure 6.2: Jeffcott Rotor Supported by Two Bearings

In this first coupling example, we are coupling a Jeffcott rotor with the Standard model, using the FAG6404 bearing. In order to achieve a realistic comparison, the stiffness of the non-linear bearing coupling is extracted from the peak of its transient analysis. That value is used as a linearization for the linear bearings coupling. When compared this way, it seems that the resonance point is almost identical. The same goes for the amplitude. It is notable that when a different linearization is used, different point of resonance and amplitude occurs. Thus, it is safe to assume that different linearization leads to different transient responses. Additionally, the general advantage of non-linear models is highlighted, as they produce stiffness that adapts to each operation. That is exceptionally useful when coupled with a rotor, as a widespread amount of stiffness is taken into consideration, directly without any linearization.

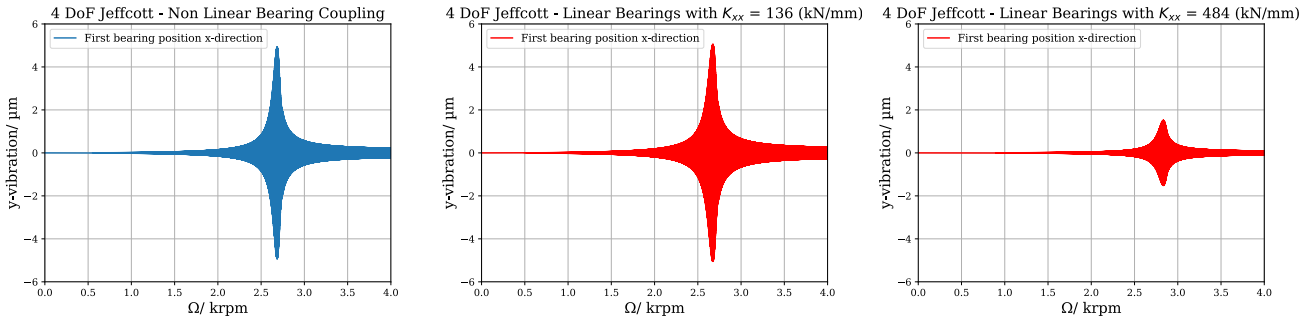

Figure 6.3: Jeffcott Rotor Transient Analysis: Comparison of Direct Coupling and Constant Bearing Stiffness Assumption

6.0.2 Realistic LP Rotor Example

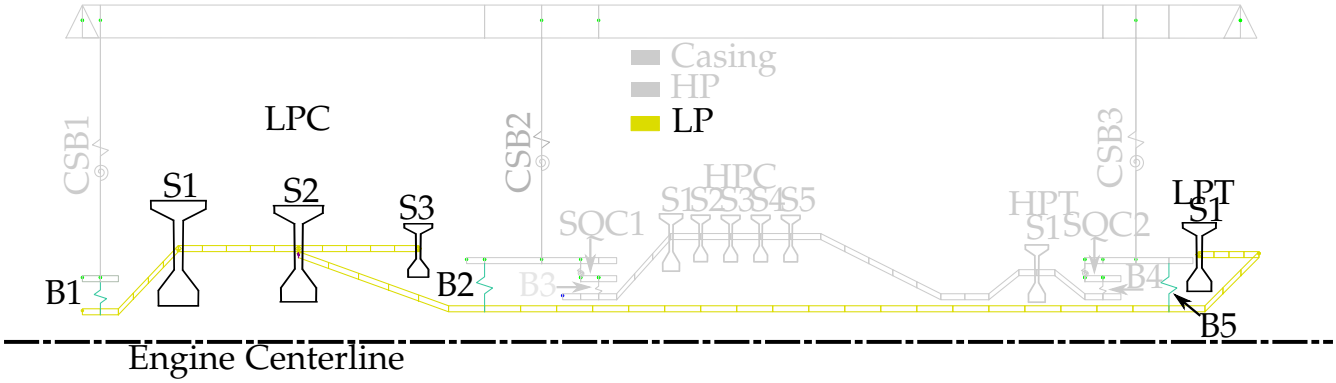

Figure 6.4: Realistic Engine [20]

For this example, a realistic Low Pressure (LP) Rotor is used (see figure 6.4). This part of the rotor was taken from a dual spool engine. Then, the High Pressure (HP) part of the rotor is deactivated, including the casing. That leaves the LP part and the three bearings, in the positions B1, B2, B5. For this particular example, the bearing in B2 is replaced with a non-linear model and the rest are kept as linear. However, this can change accordingly.

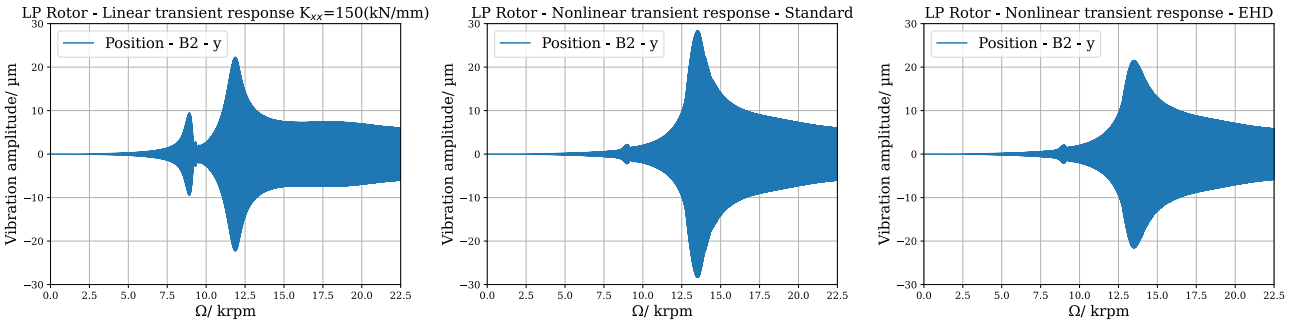

Figure 6.5: LP Rotor Transient Analysis: Comparison Between Constant Bearing Stiffness and Direct Coupling of Standard (LS) and EHD model

The coupling is done like the Jeffcott example. However in this case, a reduction has to be done. In this case the Guyan reduction is used. The time domain (transient) analysis is done using the "Backward Differentiation Formula" (BDF). Here, a typical aircraft engine ball bearing is used. The system is again slightly damped, using the same Rayleigh coefficients 6.3. The rotational speed of the rotor goes through 0 to 22.5 $krpm$. For this comparison, the Standard and the EHD models are used, to reduce the computational time. In regards of the Full model, it takes more time to execute the dynamic equilibrium. For the linear model, a basic bearing linearization is used. It is evident that two resonance peaks occur. Regarding the linearization, it could have been done by running the non-linear model, extract the stiffness at the resonance peaks and conduct the linearization with different coefficients. However, this is time consuming and it defeats the purpose of this analysis. Additionally, this highlights further the need of a non-linear bearing model, that produces the stiffness matrix without any linearization assumption, like it is done here. Moving forward to the Standard model, two resonance peaks occur.

The peaks are around the same magnitude scale as the linear one, but still remain quite different, especially in the first peak. The first peak seems exceptionally more damped. Also, the resonance has moved to the right in general. The EHD model, displays the same behaviour. However the system is more damped, as the lubrication produces some damping. It must be noted that the effect after the resonance is caused by a transient sweep [10] and can be adjusted by changing the parameters of the solver.

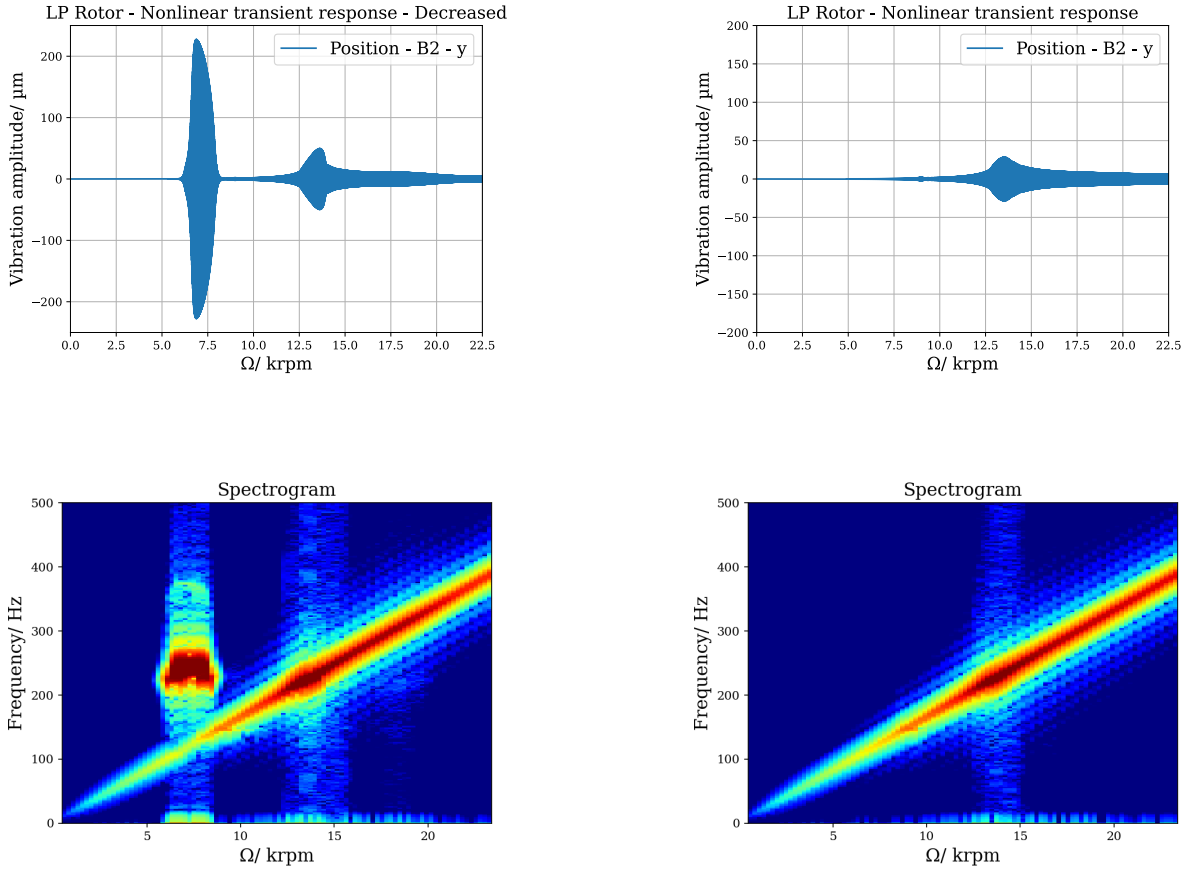

Figure 6.7: Transient Analysis Comparison between Normal and Decreased Rayleigh Damping

While keeping the same problem configuration, this time the Rayleigh damping is reduced to half as before. When doing that, an interesting phenomena occurs. It seems that a self excitation occurs and a different mode appears. To further analyse this, a spectrogram has been made. From that it is clearly evident that a separate is introduced, one that is in a higher frequency than the unbalance. This may be caused because of the bifurcation. It seems not to be a numerical phenomenon, as it showcases the same behaviour when used a different solver.

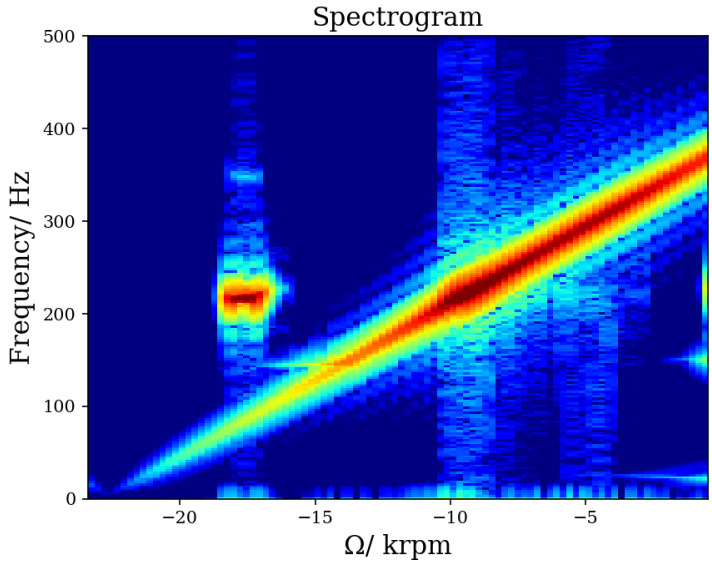

Figure 6.8: Transient Analysis Rundown with a Decreased Rayleigh Damping

Further more, even when performing a run-down, we experience the same behaviour in this case. For this excitation to be diminished, additional damping must be deployed, or increase the Rayleigh damping in this case. Therefore, we can conclude that this phenomenon is based on physical occurrences that must be investigated further. It is clearly shown that the displacement of the bearing is great and most likely to cause contact in the different parts of the machine. Thus it is essential for this to be investigated, because in the future, ball bearings may be used to replace the squeeze film dampers (SFD). Ball bearings may prove to be more financially beneficial, as they need less lubrication to operate. When using an SFD this phenomenon doesn't occur, as the damping is greater. Thus we can once again assume that it is an occurrence because of the damping. In order to determine the cause of that, a parameter investigation of each element of the whole system must be done, but this is not the premise of this thesis. However, it is a topic worthwhile of investigation.

7 Conclusion

This thesis has succeeded in presenting the stand alone non-linear bearing models, that can be used for a variety of applications. From the basic kinematic modelling, using analytic expressions to deduce results while using only dry contact, to dynamic models that implement the dynamic equilibrium, gyroscopic and centrifugal phenomena. According the computational power and time available, only dry models can be used for calculations or add the elastohydrodynamic effect (EHD). This effect was modelled according to available approximations, however even more detailed modelling can be achieved, by investigating further the Reynolds equation and the calculation of the elliptic integrals. In addition, this thesis brought to light the relation between the kinematics and the stress. The different results that were produced by exploring different kinematic configurations was presented. This proposes that we can achieve even more accurate results when the kinematic relations of the bearing is even more realistically expressed. Furthermore, this work can be further expanded by integrating into the modelling the different thermal effects that take place during bearing operation, as well as skidding effects, different press fits and the centrifugal expansion of rings.

A race control hypothesis was also introduced. This is one open topic for investigation, as the formulation of the race control can even more accurately represent the tangential force transfer between the two races. It is worthwhile to also formulate λ, such as to take into consideration lubrication cases too. Thus affecting differently the equilibrium. Using the race control with the updated kinematics we can achieve close results to the ADORE data, suggesting that ,in low rotational speed, the model is validated. For high rotational speed however, race control needs to be investigated further. In addition of these stand alone models, it cannot be undermined, that all models indicate a non-linearity in regards to stiffness, when tested for both speed or load dependency. This proves to be very important for jet engine applications, as such operations have high thrust loads, affecting the bearing's stiffness.

In addition, the findings of this research indicate that there is a relation between the non-linearity of bearings to the overall behaviour of a rotor system. Assessing the different effects that occur when coupling the non-linear bearings to a rotor, bifurcation occurs. This interesting self excitation, needs to be further investigated, as it seems to have a correlation to the damping system of the rotor. Finally, this thesis showcases how the non-linear bearings can be coupled directly to a rotor, producing results, without the need of a linearization, while unveiling phenomena that wouldn't be detectable by using a linear model. In general, this work proves that there is a vast usage of these tools and they can be further improved to serve even more in the field of rotordynamics.

Finally, the main suggestions for future work to improve the ball bearing modelling consist of:

- Improved Implementation of Race Control Hypothesis

- More Detailed Implementation of EHD Contacts
- Thermal Effects
- Centrifugal Expansion of the Rings
- Press Fits
- Skidding Criteria

8 Appendix

8.1 Varying Velocity

In this part of the thesis, the case of an input of varying velocity is investigated. The displacement vector of the inner ring u is set to zero and only velocity $\dot{u}$ is given. The purpose here is to see the relation between the velocity and the output. The same expressions are used as the EHD inverse problem. Thus, it is expected to have a constant stiffness and a linear force as the velocity is used only as part of the partial derivation as seen on section (2.3.3):

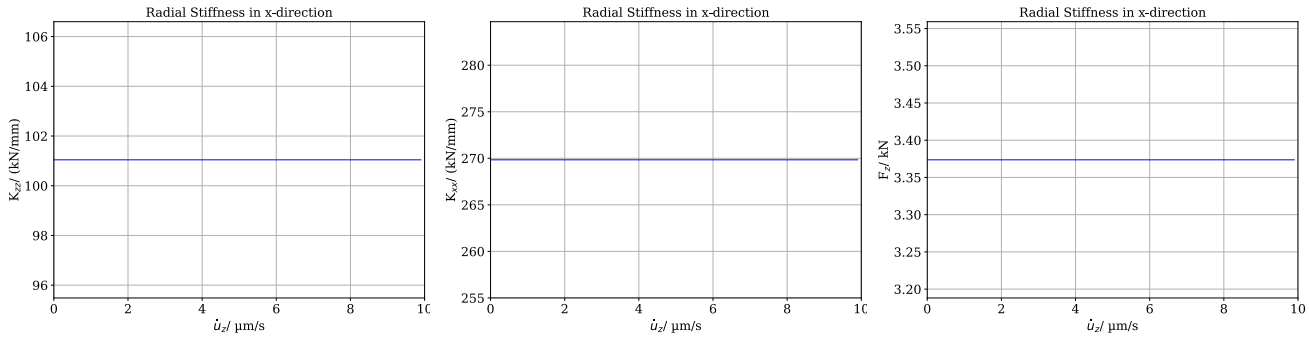

Figure 8.1: EHD Varying Velocity and Constant Displacement

8.2 Influence of Viscosity to EHD Damping Coefficient

In the following example, two different formulations are used to showcase this relation. Here, a comparison is done between the Wensing [28] and Wagner [26] formulation of damping. Here the EHD model is used, which takes into account the damping coefficients and viscosity and we vary the dynamic viscosity h_0 for values 0 to 20e-3. The bearing parameters that were used are given in section (8.3.3).

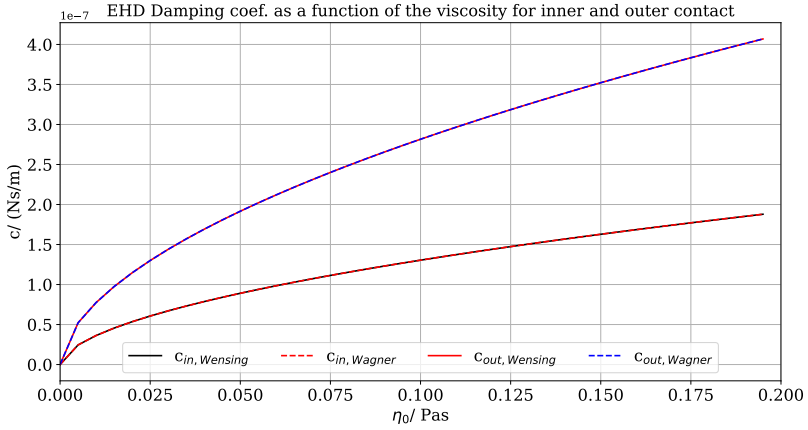

Figure 8.2: Comparison of Wensing vs. Wagner Damping coef. Calculation

Notably, the two formulations show no signs of variation and it is clear that there is an influence of the viscosity to the damping coefficient. In all the investigation, the Wagner formulation for the damping is used.

8.3 Ball Bearing Geometric and Fluid Parameters

8.3.1 FAG6404

Inner Ring

d_{in}	31.845 mm	*Raceway diameter*
D_{in}	20.000 mm	*Ring diameter*
r_{in}	7.7057 mm	*Race radius*

Outer Ring

d_{out}	62.955 mm	*Raceway diameter*
D_{out}	72.000 mm	*Ring diameter*
r_{out}	7.8239 mm	*Race radius*

Rolling Element

N	6	$Number\ of\ balls$
D_b	15.1 mm	$Diameter$

Lubricant

α_p	$1 \bullet 10^{-8} Pa^{-1}$	$Pressure - viscosity\ coefficient$
η_0	0.11 $Pa \bullet s$	$Dynamic\ viscosity\ at\ ambient\ pressure$

General

E	210 GPa	$Young's\ modulus$
ν	0.300	$Poisson's\ ratio$

References

[1] Antoine, J-F ; Abba, Gabriel ; Molinari, Alain: A new proposal for explicit angle calculation in angular contact ball bearing. (2006)

[2] Bozet, Jean-Luc ; Servais, Christophe: Influence of the balls kinematics of axially loaded ball bearings on Coulombic frictional dissipations. In: *Journal of Tribology* 139 (2017), Nr. 1, S. 011502

[3] Changan, DING ; Fuzhang, ZHOU ; Jun, Zhu ; Lei, Zhang: Raceway control assumption and the determination of rolling element attitude angle. In: *Journal of Mechanical Engineering* 37 (2001), Nr. 2, S. 58–61

[4] Friswell, Michael I.: *Dynamics of rotating machines*. Cambridge university press, 2010

[5] Gao, Shuai ; Chatterton, Steven ; Naldi, Lorenzo ; Pennacchi, Paolo: Ball bearing skidding and over-skidding in large-scale angular contact ball bearings: Nonlinear dynamic model with thermal effects and experimental results. In: *Mechanical Systems and Signal Processing* 147 (2021), S. 107120

[6] Géradin, Michel ; Rixen, Daniel J.: *Mechanical vibrations: theory and application to structural dynamics*. John Wiley & Sons, 2014

[7] Grekoussis, R ; Michailidis, Th: Näherungsgleichungen zur Nach-und Entwurfsrechnung der Punktberührung nach Hertz. (1981)

[8] Gupta, Pradeep K.: *Advanced dynamics of rolling elements*. Springer Science & Business Media, 2012

[9] Gupta, Pradeep K.: *ADORE:Advanced Dynamics Of Rolling Elements User's Guide*. 2014

[10] Hackenberg, Hans-Peter ; Hartung, Andreas: An approach for estimating the effect of transient sweep through a resonance. In: *Journal of Engineering for Gas Turbines and Power* 138 (2016), Nr. 8, S. 082502

[11] Harris, Tedric A. ; Kotzalas, Michael N.: *Essential concepts of bearing technology*. CRC press, 2006

[12] Jones, AB: Ball motion and sliding friction in ball bearings. In: *Journal of Basic Engineering* 81 (1959), Nr. 1, S. 1–12

[13] Jones, AB: A general theory for elastically constrained ball and radial roller bearings under arbitrary load and speed conditions. (1960)

[14] Krämer, Erwin: *Dynamics of rotors and foundations*. Springer Science & Business Media, 2013

[15] Kurvinen, Emil ; Sopanen, Jussi ; Mikkola, Aki: Ball bearing model performance on various sized rotors with and without centrifugal and gyroscopic forces. In: *Mechanism and Machine Theory* 90 (2015), S. 240–260

[16] Liao, Neng T. ; Lin, Jen F.: Ball bearing skidding under radial and axial loads. In: *Mechanism and Machine Theory* 37 (2002), Nr. 1, S. 91–113

[17] Liew, A ; Feng, N ; Hahn, EJ: Transient rotordynamic modeling of rolling element bearing systems. In: *J. Eng. Gas Turbines Power* 124 (2002), Nr. 4, S. 984–991

[18] Lim, Teik C. ; Singh, Rajendra: Vibration transmission through rolling element bearings, part I: bearing stiffness formulation. In: *Journal of sound and vibration* 139 (1990), Nr. 2, S. 179–199

[19] Lim, Teik C. ; Singh, Rajendra: Vibration transmission through rolling element bearings, part II: system studies. In: *Journal of sound and vibration* 139 (1990), Nr. 2, S. 201–225

[20] Mitsos, Georgios: *Influence of Speed and Eccentricity Dependent Bearing Stiffness and Damping on Rotor Vibration*, 2022

[21] Noel, David ; Ritou, Mathieu ; Furet, Benoit ; Le Loch, Sebastien: Complete analytical expression of the stiffness matrix of angular contact ball bearings. In: *Journal of Tribology* 135 (2013), Nr. 4, S. 041101

[22] Scholz, Dieter: Jet Engines–Bearings, Seals and Oil Consumption. (2021)

[23] Servais, Christophe ; Bozet, J-L: New computational method of the ball/race contacts transverse loads of high speed ball bearings without race control hypothesis. In: *Tribology International* 113 (2017), S. 206–215

[24] Servais, Christophe ; Bozet, Jean-Luc: Influence of the balls kinematics and ball/race contact models on quasi-static approaches for ball bearing. In: *STLE Annual Meeting 2016*, 2016

[25] Tiwari, M ; Gupta, K ; Prakash, O: Effect of radial internal clearance of a ball bearing on the dynamics of a balanced horizontal rotor. In: *Journal of sound and vibration* 238 (2000), Nr. 5, S. 723–756

[26] Wagner, Christian: *Dynamic Modeling of Turbopumps*, Technische Universität München, Diss., 2019

[27] Wang, Wen-zhong ; Hu, Lang ; Zhang, Sheng-guang ; Zhao, Zi-qiang ; Ai, Siyuan: Modeling angular contact ball bearing without raceway control hypothesis. In: *Mechanism and Machine Theory* 82 (2014), S. 154–172

[28] Wensing, Jeroen A.: On the dynamics of ball bearings. In: *University of Twente* (1998)

[29] Wijnant, Ysbrand H. [u. a.]: *Contact dynamics in the field of elastohydrodynamic lubrication*. Universiteit Twente Enschede, the Netherlands, 2003